HHS Public Access

Author manuscript

Circ Res. Author manuscript; available in PMC 2022 July 23.

Published in final edited form as:

Circ Res. 2021 July 23; 129(3): 349–365. doi:10.1161/CIRCRESAHA.120.318643.

Targeting the Microtubule EB1-CLASP2 Complex Modulates $Na_V1.5$ at Intercalated Discs

Gerard A. Marchal[1,*], **Mariam Jouni**[2,*], **David Y. Chiang**[3,*], **Marta Pérez-Hernández**[4,*], **Svitlana Podliesna**[1], **Nuo Yu**[5], **Simona Casini**[1], **Franck Potet**[2], **Christiaan C. Veerman**[1], **Mischa Klerk**[6], **Elisabeth M. Lodder**[1], **Isabella Mengarelli**[1], **Kaomei Guan**[7], **Carlos G. Vanoye**[2], **Eli Rothenberg**[8], **Flavien Charpentier**[9], **Richard Redon**[9], **Alfred L. George Jr.**[2], **Arie O. Verkerk**[1,6], **Connie R. Bezzina**[1], **Calum A. MacRae**[3], **Paul W. Burridge**[2], **Mario Delmar**[4], **Niels Galjart**[5], **Vincent Portero**[1,9,#], **Carol Ann Remme**[1,#]

[1]Experimental Cardiology, Amsterdam UMC – location AMC, Amsterdam, The Netherlands [2]Pharmacology, University Feinberg School of Medicine, Chicago, Illinois, USA [3]Brigham and Women's Hospital and Harvard Medical School, Boston, MA, USA [4]Division of Cardiology, NYU School of Medicine, New York, NY, USA [5]Cell Biology, Erasmus Medical Centre, Rotterdam, The Netherlands [6]Medical Biology, Amsterdam UMC, Amsterdam, The Netherlands [7]Institute of Pharmacology and Toxicology, Technische Universität Dresden, 01307 Dresden, Germany [8]Biochemistry and Pharmacology, NYU School of Medicine, New York, NY, USA [9]Université de Nantes, CNRS, INSERM, l'institut du Thorax, Nantes, France.

Abstract

Rationale: Loss-of-function of the cardiac sodium channel $Na_V1.5$ causes conduction slowing and arrhythmias. $Na_V1.5$ is differentially distributed within subcellular domains of cardiomyocytes, with sodium current (I_{Na}) being enriched at the intercalated discs (ID). Various pathophysiological conditions associated with lethal arrhythmias display ID-specific I_{Na} reduction, but the mechanisms underlying microdomain-specific targeting of $Na_V1.5$ remain largely unknown.

Address correspondence to: Dr. Vincent Portero, Department of Experimental Cardiology, Amsterdam UMC, location Academic Medical Center, Room K2-104.2 Meibergdreef 9, 1105 AZ Amsterdam, The Netherlands, Tel: +31-20-5663262, v.m.portero@amsterdamumc.nl, Dr. Carol Ann Remme, Department of Experimental Cardiology, Amsterdam UMC, location Academic Medical Center, Room K2-104.2 Meibergdreef 9, 1105 AZ Amsterdam, The Netherlands, Tel: +31-20-5663262, c.a.remme@amsterdamumc.nl.

*denotes shared first authorship

#denotes shared last authorship.

DISCLOSURES

The authors have reported that they have no relationships with industry relevant to the contents of this paper to disclose.

SUPPLEMENTARY MATERIALS

Expanded Materials & Methods

Online Figures I – XII

Online Tables I – XX

References 82 – 106

Objective: To investigate the role of the microtubule (MT) plus-end tracking proteins end binding protein 1 (EB1) and CLIP-associated protein 2 (CLASP2) in mediating $Na_V1.5$ trafficking and subcellular distribution in cardiomyocytes.

Methods and Results: EB1 overexpression in human induced pluripotent stem cell-derived cardiomyocytes (hiPSC-CMs) resulted in enhanced whole-cell I_{Na}, increased action potential (AP) upstroke velocity (V_{max}), and enhanced $Na_V1.5$ localization at the plasma membrane as detected by multi-color stochastic optical reconstruction microscopy (STORM). Fluorescence recovery after photobleaching (FRAP) experiments in HEK293A cells demonstrated that EB1 overexpression promoted $Na_V1.5$ forward trafficking. Knockout of *MAPRE1* in hiPSC-CMs led to reduced whole-cell I_{Na}, decreased V_{max} and AP duration (APD) prolongation. Similarly, acute knockout of the *MAPRE1* homolog in zebrafish (*mapre1b*) resulted in decreased ventricular conduction velocity and V_{max} as well as increased APD. STORM imaging and macropatch I_{Na} measurements showed that subacute treatment (2–3 hours) with SB216763 (SB2), a GSK3β inhibitor known to modulate CLASP2-EB1 interaction, reduced GSK3β localization and increased $Na_V1.5$ and I_{Na} preferentially at the ID region of wild type murine ventricular cardiomyocytes. By contrast, SB2 did not affect whole cell I_{Na} or $Na_V1.5$ localization in cardiomyocytes from *Clasp2*-deficient mice, uncovering the crucial role of CLASP2 in SB2-mediated modulation of $Na_V1.5$ at the ID.

Conclusions: Our findings demonstrate the modulatory effect of the MT plus-end tracking protein EB1 on $Na_V1.5$ trafficking and function, and identify the EB1-CLASP2 complex as a target for preferential modulation of I_{Na} within the ID region of cardiomyocytes.

Graphical Abstract

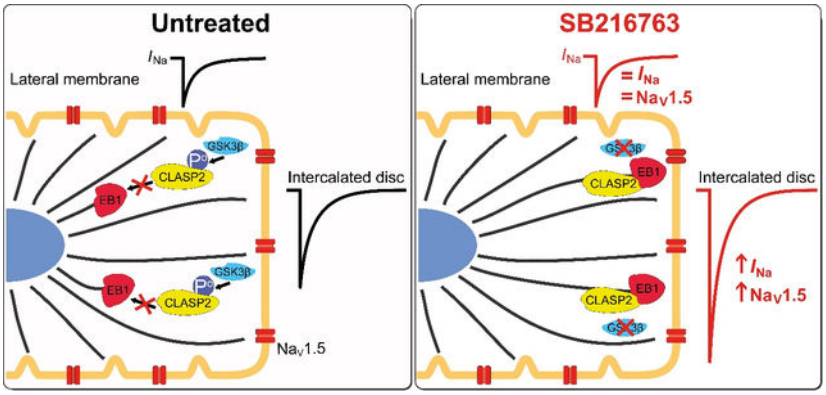

Keywords

$Na_V1.5$; microtubule; trafficking; electrophysiology; intercalated discs; cardiomyocyte; Na+ current; Arrhythmias; Ion Channels/Membrane Transport

INTRODUCTION

The cardiac voltage-gated sodium channel $Na_V1.5$ mediates the fast upstroke of the cardiac action potential, driving cardiomyocyte excitability and enabling proper cardiac conduction. Loss of $Na_V1.5$ function, either acquired or inherited, is associated with cardiac conduction

slowing, a well-established risk factor for arrhythmias and sudden cardiac death.[1,2] $Na_V1.5$ displays differential distribution and functionality within cardiomyocyte microdomains, such as the lateral membrane and intercalated disc (ID), where it interacts with distinct sets of proteins.[3,4] Moreover, $Na_V1.5$ is differentially regulated in a microdomain-specific manner in the setting of acquired and inherited conditions such as heart failure and arrhythmogenic cardiomyopathy.[5,6] However, the mechanisms underlying subcellular, microdomain-specific targeting of $Na_V1.5$ remain largely unknown, which prevents the development of novel strategies aimed at restoring excitability.

The microtubule (MT) network is essential for targeting proteins to the plasma membrane.[7] This process is tightly regulated by MT plus (+)-end tracking proteins, which attach to the growing end of MTs and thereby modulate MT dynamicity and function.[8] In neurons, networks of MT (+)-end tracking proteins are responsible for the delivery of ion channels to specific subcellular domains. Among the MT (+)-end tracking proteins, end binding protein 1 (EB1) mediates the subcellular localization of sodium and potassium channels at the axon initial segment and Ranvier nodes.[9–11] Furthermore, EB1 has been demonstrated to be essential for the targeted delivery of the gap junction protein connexin-43 (Cx43) to adherens junctions.[12,13] During oxidative stress, EB1 is displaced from MT (+) ends, limiting both MT growth and forward trafficking of Cx43 to the plasma membrane.[13] In cardiomyocytes, EB1 is mainly observed at the ID,[13] where $Na_V1.5$ and Cx43 are both enriched. EB1, Cx43, and $Na_V1.5$ are jointly removed from the ID in adult sheep right ventricular cardiomyocytes following right ventricular pressure overload and in mice carrying a non-sense mutation in Cx43,[14,15] suggesting a possible modulatory role for EB1 in subcellular distribution of $Na_V1.5$.

MTs undergo dynamic physiological switching between growth and shrinkage states.[7] At the MT (+) end, EB1 enhances MT dynamicity and promotes MT elongation.[16–18] Additionally, EB1 facilitates tethering of MTs to specific cellular structures in several cell types,[9,12] potentially enhancing ion channel trafficking and anchoring.[14] The interaction of EB1 with cytoplasmic linker associated protein 2 (CLASP2) at the MT (+) end also facilitates MT polymerization and stabilization.[19–21] This interaction is increased by inhibition of glycogen synthase kinase 3β (GSK3β)-mediated phosphorylation of CLASP2, as previously demonstrated in COS-7 cells using the compound SB216763 (SB2), a GSK3β-inhibitor.[22–24] In a chemical screen of a zebrafish model of arrhythmogenic cardiomyopathy, where a human mutant plakoglobin was transgenically expressed, SB2 was found to suppress the mutant phenotype. In particular, SB2 restored the global loss of sodium current (I_{Na}) observed in this model without increasing available sodium channel protein; however, the underlying mechanism and potential microdomain-specific effects on I_{Na} were not investigated.[25]

In this study we investigate the role of the MT (+)-end tracking EB1-CLASP2 protein complex on $Na_V1.5$ trafficking, subcellular distribution and function in cardiomyocytes. We provide evidence that EB1 mediates I_{Na} and cardiac conduction, and demonstrate that SB2 modulates $Na_V1.5$ and I_{Na} preferentially at the ID of cardiomyocytes in a CLASP2-dependent manner. In addition to demonstrating a crucial role for MT (+)-end tracking

proteins in modulating I_{Na}, our findings identify the EB1-CLASP2 protein complex as a target for preferential modulation of I_{Na} in cardiomyocyte subcellular domains.

METHODS

Data Availability.

A description of all materials and methods is provided in the Online Data Supplement and are available from the corresponding author upon reasonable request.

RESULTS

EB1 overexpression increases I_{Na} density and AP upstroke velocity in hiPSC-CMs.

The impact of EB1 overexpression on $Na_V1.5$ plasma membrane localization, I_{Na} and upstroke velocity was investigated in human induced pluripotent stem cell-derived cardiomyocytes (hiPSC-CMs) transduced with lentiviral vectors containing either EB1-IRES-GFP or GFP. As expected, increased mRNA levels of *MAPRE1* encoding EB1 were observed in hiPSC-CMs transduced with EB1-IRES-GFP lentivirus as compared to cells transduced with the GFP empty vector and untransduced cells, without changes in mRNA expression of *SCN5A* encoding $Na_V1.5$ (Online Fig. I). Expression of *STAT1*, encoding signal transducer and activator of transcription 1, also remained unchanged among the three groups, indicating absence of interferon response after virus transduction. Fig. 1A–C depicts representative I_{Na} traces, current-voltage (*I-V*) relationships, and I_{Na} density at −20 mV measured in hiPSC-CMs transduced with EB1-IRES-GFP or GFP only (GFP-control). We observed a significantly greater I_{Na} density in hiPSC-CMs overexpressing EB1 compared to GFP-control hiPSC-CMs and a slight hyperpolarizing shift of voltage-dependence of activation, without changes in the voltage-dependence or time course of inactivation (Online Table I). We further explored the electrophysiological effects of EB1 overexpression through current clamp experiments in hiPSC-CMs employing inward rectifier potassium current (I_{K1}) dynamic clamp injection (with Kir2.1 kinetics).[26] In line with the observed increase in I_{Na}, maximum action potential (AP) upstroke velocity (V_{max}) was significantly higher in hiPSC-CMs with EB1 overexpression compared to GFP-control hiPSC-CMs. EB1 overexpression did not significantly affect AP amplitude (APA), resting membrane potential (RMP), or AP duration at 20, 50, or 90% repolarization (APD_{20}, APD_{50}, APD_{90} respectively) (Fig. 1D,E; Online Table II).

EB1 overexpression increases plasma membrane $Na_V1.5$ cluster density in hiPSC-CMs and enhances $Na_V1.5$ membrane trafficking in HEK293A cells.

I_{Na} magnitude is determined by the density and size of $Na_V1.5$ clusters at the cell membrane.[27] To assess the impact of EB1 on $Na_V1.5$ cluster properties, we applied multi-color stochastic optical reconstruction microscopy (STORM), a super-resolution approach,[18] on fixed hiPSC-CMs. Fig. 1F displays STORM images with immunoreactive signals for $Na_V1.5$ (green) and N-cadherin (red) in EB1-IRES-GFP or GFP transduced hiPSC-CMs. In total, 871 clusters from 55 images of GFP transduced cells and 2866 clusters from 102 images of EB1-IRES-GFP cells were included in the analysis. As shown in Fig 1G, $Na_V1.5$ cluster density in hiPSC-CMs upon EB1 overexpression was significantly increased

compared to GFP-control hiPSC-CMs, whereas $Na_V1.5$ cluster size was not significantly different between conditions. Neither N-cadherin cluster density nor N-cadherin cluster size were affected by EB1 overexpression (Fig. 1G; Online Table III). Moreover, the average distance between $Na_V1.5$ and N-cadherin clusters as well as the distance distribution was similar in GFP-control and EB1-IRES-GFP hiPSC-CMs (Online Fig. II; Online Table III).

Similar to observations in hiPSC-CMs, co-expression of $Na_V1.5$+$Na_V\beta1$ with EB1 in HEK293A cells (which express EB1 endogenously; Online Fig. IIIA) led to a significant increase in I_{Na} (Online Fig. IIIB–D), without affecting the voltage dependence of activation or inactivation (Online Table IV). To assess the impact of EB1 on $Na_V1.5$ trafficking, we performed fluorescence recovery after photobleaching (FRAP) in HEK293A cells transfected with N-terminally GFP-fused $Na_V1.5$ (GFP-$Na_V1.5$) with or without *MAPRE1*/EB1. Following bleaching, GFP-$Na_V1.5$ fluorescence was continuously recorded at a frequency of 2 Hz for a 75-second period (Fig. 1H,I). The fluorescence signal was fitted using an exponential plateau fit ($Y = Y_M - (Y_M - Y_0) \times \exp(-kt)$) where Y_M represents the maximum fluorescence recovery signal, Y_0 the lowest fluorescence intensity, and k the speed of recovery after photobleaching. Similar FRAP recordings were also performed after 2-hour incubation with paclitaxel (10 μmol/L), an anticancer drug known to suppress MT dynamics[28] and decrease I_{Na}.[29] While k values remained unchanged between groups, paclitaxel significantly decreased the maximum GFP-$Na_V1.5$ fluorescence recovery signal following bleaching. In contrast, co-expression of EB1 with GFP-$Na_V1.5$ resulted in a significantly higher maximum fluorescence recovery signal as compared to GFP-$Na_V1.5$ alone (Fig. 1H,I; Online Table V). Taken together, these findings indicate that EB1 overexpression increases I_{Na} by enhancing $Na_V1.5$ trafficking.

Knockout of EB1 leads to reduced I_{Na} and V_{max}, APD prolongation, and ventricular conduction slowing.

To further establish the modulatory effects of EB1 on I_{Na}, we next generated *MAPRE1*/EB1 knockout (EB1-KO) hiPSC. As expected, *MAPRE1* transcripts were abolished in the EB1-knockout hiPSC-CMs without affecting *SCN5A* mRNA expression (Online Fig. IV). On patch clamp analysis, EB1-KO hiPSC-CMs showed a significant decrease in peak I_{Na} in addition to a hyperpolarizing shift in steady-state inactivation and a slower time course of inactivation, while activation kinetics were unaffected (Fig. 2A–C; Online Table VI). AP measurements, performed by setting the RMP to −80 mV with a holding current, revealed a decreased V_{max} in EB1-KO hiPSC-CMs (Fig. 2D,E; Online Table VII), in line with the observed reduced I_{Na}. While the maximal diastolic potential (MDP; measured in the absence of the holding current) and APA remained unchanged, EB1-KO hiPSC-CMs showed prolonged APD_{30}, APD_{50}, and APD_{90} (Fig. 2D,E; Online Table VII). Accordingly, total outward current ($I_{outward}$) was significantly lower in EB1-KO hiPSC-CMs, which was largely due to a reduction in E-4031-sensitive current (reflecting the rapid delayed rectifier potassium current, I_{Kr}) rather than a JNJ-303-sensitive current (reflecting the slow delayed rectifier potassium current, I_{Ks}) (Online Fig. V; Online Table VIII).

To assess the role of EB1 *in vivo*, we generated an EB1 loss-of-function model by knocking out EB1 using a multi-guide RNA (gRNA) CRISPR/Cas9 approach in zebrafish embryos.

Of the two paralogous EB1-encoding genes *mapre1a* and *mapre1b,* the latter is the dominant paralog in embryonic zebrafish heart (Online Fig. VI).[30] Therefore, we targeted *mapre1b*/EB1 with 3 different gRNAs and achieved ~50% knockout of *mapre1b* without changes in the mRNA levels of other genes in the same family (Online Fig. VIIA), or of major cardiac ion channel genes (Online Fig. VIIB). Acute knockout of *mapre1b* (EB1-KO) did not affect embryonic mortality at 24 hour post-fertilization (hpf, data not shown), heart rate and contractile function at 54 hpf, or cardiac dimensions and sizes at 3 day post-fertilization (dpf; Online Fig. VIII,IX; Online Tables IX,X). At 3 dpf, hearts were isolated and underwent optical mapping using a voltage-sensitive dye. Compared to control hearts, acute EB1-KO hearts exhibited a significantly reduced conduction velocity (CV) and AP V_{max} in the ventricle (Fig. 2F,G; Online Table XI). Furthermore, there was a significant increase in the ventricular APD_{80} in the acute EB1-KO hearts when paced at 80 bpm (Fig. 2F,G).

Ventricular Mapre1/EB1 expression correlates with QRS duration in an F2 murine progeny.

To further explore the potential functional relevance of EB1 *in vivo*, we analysed existing microarray and ECG data from a conduction disease-sensitized F2 mouse population (n = 109).[31,32] These F2 mice were generated from an intercross of two separate mouse strains carrying the *Scn5a-1798insD* mutation, which we have previously shown to display variable conduction disease severity secondary to the mutation.[33] Ventricular transcript levels of *Mapre1* encoding EB1 were negatively correlated with QRS duration ($P = 0.000118$, rho = −0.34433; Spearman non-parametric correlation; Online Fig. X) and QT duration ($P = 0.049$, rho = −0.18; Spearman non-parametric correlation), but not with QT duration corrected for heart rate (QTc). Multiple regression analysis showed that only QRS-duration was independently correlated with *Mapre1* transcript levels in ventricle.

Targeting the MT (+)-end protein complex by the GSK3β inhibitor SB216763 modulates I_{Na} in a CLASP2-dependent manner.

Having identified a clear modulatory effect of EB1 on $Na_V1.5$ and I_{Na}, we next explored the potential of targeting MT (+)-end tracking proteins. The regulatory effects of EB1 on MT dynamics and consequent cargo delivery to the membrane are facilitated by its interaction with other (+)-end tracking proteins such as CLASP2. The compound SB216763 (SB2), annotated as a GSK3β inhibitor, has been previously shown to promote the interaction between EB1 and CLASP2, thereby stabilizing MTs and potentially promoting cargo transport across MTs.[22,34] Therefore, we investigated the (sub)acute effects of SB2 on I_{Na} by incubating isolated wild type (WT) adult left ventricular murine cardiomyocytes for 2–3 hours with either SB2 (5 μmol/L) or DMSO (vehicle control). As shown in Fig. 3A–C, incubation with SB2 resulted in an approximately 30% increase in whole-cell peak I_{Na} compared to vehicle control, without affecting I_{Na} kinetics (Online Table XII). To investigate whether this effect of SB2 on I_{Na} depends on CLASP2, we repeated the experiment using *Clasp2* knockout mice (*Clasp2*$^{-/-}$). No significant baseline differences in I_{Na} were observed between WT and *Clasp2*$^{-/-}$ ventricular cardiomyocytes. However, SB2 had no effect on I_{Na} density (Fig. 3D–F) nor kinetics in *Clasp2*$^{-/-}$ cardiomyocytes (Online Table XIII). These observations indicate that modulation of the MT (+)-end tracking EB1-CLASP2 protein complex by SB2 enhances I_{Na}, and this process is crucially dependent on CLASP2.

SB2 reduces GSK3β and increases $Na_V1.5$ and I_{Na} preferentially at the ID of cardiomyocytes.

Since EB1 and CLASP2 are known to modulate MT dynamics at adherens junctions,[12,35,36] and are enriched at the ID of cardiomyocytes (Online Fig. XI),[4] we hypothesized that modulation of the MT (+)-end tracking complex by SB2 would impact $Na_V1.5$ and I_{Na} preferentially within the ID. To explore the impact of SB2 on the molecular organization of $Na_V1.5$ at a subcellular level, we performed STORM microscopy in adult ventricular cardiomyocytes from WT and *Clasp2*$^{-/-}$ mice, assessing $Na_V1.5$ cluster size and density in the lateral membrane and ID.[10] In WT cardiomyocytes, SB2 increased $Na_V1.5$ cluster size and density at the ID, but not at the lateral membrane (Fig. 4A,C; Online Table XIV). By contrast, SB2 did not affect $Na_V1.5$ cluster size or density at the ID or at the lateral membrane in cardiomyocytes from *Clasp2*$^{-/-}$ mice (Fig. 4B,D; Online Table XV), in line with the absence of effect of SB2 on whole-cell I_{Na} observed in these cells. Since SB2 has been annotated as a GSK3β inhibitor, we performed STORM analysis of GSK3β in murine adult cardiomyocytes (47 untreated cells and 58 treated cells; from N = 4 mice) and found that SB2 significantly decreased GSK3β cluster size and density at the ID (Fig. 5A,B; Online Table XVI). This was accompanied by a larger fraction of detyrosinated MTs, as indicated by an increased labelling of glu-tubulin (representing detyrosinated tubulin) and decreased levels of alpha-tubulin (total tubulin) (Fig. 5C–F; Online Table XVII).

To confirm the subdomain-specific functional impact of SB2, we performed macropatch (cell attached voltage clamp) measurements to assess I_{Na} specifically at the lateral membrane and ID region. As shown in Fig. 6A–C and Online Table XVIII, SB2 did not affect I_{Na} density or kinetics at the lateral membrane. By contrast, SB2 treatment resulted in a substantial I_{Na} increase at the ID region (Fig. 6D–F) without significant alterations in current kinetics (Online Table XIX). Hence, aside from the previously described GSK3β inhibition properties of SB2,[37] these findings indicate that targeting the MT (+)-end tracking complex by SB2 reduces the presence of GSK3β at the ID, thereby increasing $Na_V1.5$ and I_{Na} preferentially in this subcellular domain of the cardiomyocyte (Fig. 7).

DISCUSSION

In this study, we demonstrate that the MT (+)-end tracking protein EB1 regulates $Na_V1.5$ trafficking, I_{Na} and ventricular conduction. We show that modulation of the EB1-CLASP2 complex affects $Na_V1.5$ and I_{Na} preferentially at the ID, and confirm that this modulatory effect is crucially dependent on CLASP2. Taken together, our findings identify MT (+)-end tracking proteins, in particular the EB1-CLASP2 complex, as novel modulators of $Na_V1.5$ and I_{Na} within distinct subcellular domains.

In cardiomyocytes, $Na_V1.5$ is distributed heterogeneously across subcellular domains and forms macromolecular complexes with microdomain-specific interacting proteins. At the lateral membrane, $Na_V1.5$ interacts with the syntrophin-dystrophin complex, and both loss of dystrophin and disruption of the $Na_V1.5$-syntrophin interaction have been shown to decrease I_{Na} in this subcellular domain and cause cardiac conduction slowing.[38–40] Similarly, disruption of the ID-localized interacting proteins plakophilin-2 (PKP2) and coxsackie- and adenovirus receptor (CAR) reduces I_{Na} specifically at the ID.[1,41] Because

I_{Na} is larger at the ID than at the lateral membrane,[42] loss of $Na_V1.5$ at the ID results in a larger reduction of whole-cell I_{Na} and is consequently more detrimental to cardiac conduction. Additionally, $Na_V1.5$ and the β1 subunit are required for proper cell adhesion at the ID,[27,43] which is important for normal and ephaptic conduction[44,45] Hence, maintaining proper $Na_V1.5$ localization and function at the ID is crucial for preventing cardiac conduction slowing and arrhythmogenesis.

The MT network is known to form “highways” along which the motor proteins kinesin and dynein move cargo to and from the cell membrane,[7] including connexins and ion channels.[9,12,14,29,46] The significance of the MT network for the targeting of ion channels to the plasma membrane has been demonstrated in studies using agents affecting MT structure.[29,47–50] In particular, we previously demonstrated that treatment with paclitaxel, an anticancer drug known to suppress MT dynamics,[28,51] reduced $Na_V1.5$ surface expression and I_{Na}, and modified $Na_V1.5$ gating properties.[29] In addition to a modulatory effect on MT dynamics, the observed reduction in I_{Na} may also be consequent to displacement of the MT (+)-end tracking protein EB1 from MT tips, an established consequence of paclitaxel treatment.[16] EB1 participates in the dynamic stabilization of MTs by promoting their elongation, and furthermore establishes MT capture sites on the cell membrane by interacting with other proteins,[17,18,52] thereby providing anchoring points for targeted delivery of $Na_V1.5$.[14] Accordingly, our current findings show that EB1 regulates $Na_V1.5$ membrane cluster density, $I_{Na,}$ and AP upstroke velocity. Additionally, the FRAP data obtained in HEK293A cells indicate that EB1 enhances forward trafficking of $Na_V1.5$. Although no effect on the speed of recovery after photobleaching was observed upon EB1 overexpression, the higher plateau level likely reflects an enhanced vesicular transport of $Na_V1.5$. While HEK293A cells lack certain proteins and other ion channels modulating $Na_V1.5$ function and trafficking,[53,54] we observed a clear similarity in patch clamp data obtained from HEK293A cells and hiPSC-CMs overexpressing EB1. Additionally, our FRAP data in HEK293A cells are consistent with our STORM imaging and patch clamp findings in hiPSC-CMs showing increased $Na_V1.5$ membrane localization and I_{Na}. Conversely, knockout of *MAPRE1*/EB1 in hiPSC-CMs greatly reduced I_{Na} density, underlining its crucial role in $Na_V1.5$ trafficking. Interestingly, EB1 knockout also impacted I_{Na} inactivation properties, indicating this MT (+)-end tracking protein may also modulate channel kinetics, possibly by affecting the $Na_V1.5$ macromolecular complex.

The *in vivo* functional relevance of EB1 and its impact on I_{Na} was demonstrated by our findings in zebrafish where acute EB1 knockout led to a decrease in ventricular V_{max} and conduction velocity. The negative correlation between ventricular EB1 expression and QRS duration observed in *Scn5a*-1798insD F2 mice further underscores the role of EB1 on ventricular conduction in adult hearts. Conversely, the APD prolongation observed in both the hiPSC-CMs and zebrafish EB1 knockout models suggest an additional impact on repolarization, which was confirmed by a reduction in the E-4031-sensitive outward current (representing I_{Kr}) following EB1 knockout in hiPSC-CMs. This is in line with previous observations that EB1 modulates the subcellular trafficking of both sodium and potassium channels in the axon initial segment of neurons.[55] A recent study also demonstrated an essential role for the MT network in modulating the ultrarapid delayed rectifier potassium channel ($K_V1.5$) trafficking in atrial cardiomyocytes, demonstrating that mobile $K_V1.5$

channels were predominantly associated with EB1.[56] Hence, the role of the MT network and the MT (+)-end binding complex in subcellular targeting of ion channels extends beyond effects on $Na_V1.5$. Whether the impact on other ion channels is consequent to a direct modulatory effect or through an indirect effect on co-trafficking of e.g. sodium and potassium channels,[57] deserves future exploration.

In adult cardiomyocytes, EB1 was previously detected primarily at IDs.[14,15] In HeLa cells, EB1 was shown to be directly involved in the targeting of Cx43 to the cell-cell border through MT interaction with adherens junctions.[12] Moreover, decreased EB1 localization at the ID as a result of right ventricular pressure overload[15] and in the setting of Cx43 C-terminus truncation[14] was associated with changes in $Na_V1.5$ distribution and I_{Na}, suggesting a possible role for EB1 in targeting $Na_V1.5$ to the ID.[14,15] These findings are in line with studies in neurons, where the interaction between EB proteins and ankyrin-G is crucial for localization of both ankyrin-G and sodium channels at the neuronal axon initial segment.[10,11] In addition to ankyrin-G, which has previously been shown to be essential for the anchoring of $Na_V1.5$ at the ID of cardiomyocytes,[58,59] EB1 associates with the ID proteins desmoplakin[60] and p150 (Glued), as well as dynein intermediate chain and dynamitin[35] which are part of the dynactin/dynein complex.[61] Additionally, the MT (+)-end tracking protein CLASP2 has been shown to interact with the ID protein p120-catenin, thereby governing MT dynamics at adherens junctions.[36,62] These interactions of MT (+)-end tracking proteins with ID-specific proteins may be facilitating MT anchoring and subsequent $Na_V1.5$ delivery to this specific subcellular domain.[14]

In our experiments, overexpression of EB1 in hiPSC-CMs induced a significant increase in $Na_V1.5$ cluster size in regions of cell-to-cell contact, defined as areas with enrichment of N-cadherin. Although hiPSC-CMs do not possess a mature subcellular organization similar to adult cardiomyocytes, they do have intercellular junctions and $Na_V1.5$ preferentially localizes to these regions of cell-to-cell contact (although not exclusively). Accordingly, hiPSC-CMs have previously been successfully employed to investigate $Na_V1.5$ (dys)function and model diseases associated with alterations in the ID region, including arrhythmogenic cardiomyopathy (ACM).[25,41,63] While our findings in hiPSC-CMs indicate an effect of EB1 on $Na_V1.5$ in the “ID-like” region, we cannot completely exclude an effect of EB1 on $Na_V1.5$ in the lateral membrane because the relative immaturity of hiPSC-CMs precludes accurate assessment of this subcellular domain. However, our results in mouse cardiomyocytes show that SB2, which is known to modulate EB1-CLASP2 interaction,[22] does not affect $Na_V1.5$ or I_{Na} at the lateral membrane.

Inherited disorders characterized by reduced I_{Na} and conduction disturbances such as Brugada syndrome (BrS) and ACM still lack effective therapeutic options. ACM is typically caused by mutations in desmosomal proteins, and studies in ACM murine models have shown that gap junction remodelling[64,65] and I_{Na} reduction[25,65–68] may precede the development of cardiac structural abnormalities and ventricular arrhythmias.[64–66] Decreased levels of $Na_V1.5$ and Cx43 at the ID have been demonstrated in patients with ACM,[5,64,69–71] and certain ACM mutations have been shown to lead to mis-localization of EB1 and impairment of MT dynamics.[60] Heterozygous deletion of the desmosomal protein PKP2 in cardiomyocytes caused both a reduction in I_{Na} and a separation of MT (+) ends (marked by

EB1) from N-cadherin plaques at the ID, indicating that the latter may have impaired protein delivery to the cell membrane.[41] Given the well-established pro-arrhythmic consequences of decreased $Na_V1.5/I_{Na}$, development of novel pharmacological interventions to restore their levels is crucial.

Recently, a chemical screen identified a novel compound which restored I_{Na} in both a zebrafish ACM model and neonatal rat ventricular cardiomyocytes expressing mutant desmosomal protein plakoglobin.[25] This compound, SB216763 (SB2), has been annotated as a GSK3β inhibitor.[37] In fibroblasts and epithelial cells, GSK3β-mediated phosphorylation of the MT (+)-end tracking protein CLASP2 was shown to inhibit CLASP2 interactions with EB1 and MTs, while SB2 treatment re-established EB1 and CLASP2 colocalization and CLASP2 accumulation on MTs.[22,23] Additionally, previous research revealed that facilitation of GSK3β phosphorylation by agrin is crucial for CLASP2-mediated neuromuscular junction formation.[72] Hence, GSK3β significantly impacts the function of CLASP2, which is a selective MT stabilizer that reduces the rapid breakdown of MTs (i.e. MT catastrophe) in specific cellular domains.[19,20,73] Additionally, CLASP2 is involved in the establishment of focal adhesions in various cell types and the formation of the neuromuscular junction.[72,74] EB1 has been shown to be enriched at the ID by immunohistochemistry in cardiac tissue,[13,15] and CLASP2 has recently been identified as putative ID-specific proteins by mass spectrometry studies in cardiomyocytes,[75] Additionally, CLASP2 is known to interact with p120-catenin which is specifically localized at the ID in cardiomyocytes.[36] Based on these observations, we hypothesized that SB2 enhances EB1-CLASP2 and MT-CLASP2 interactions, and thereby facilitates the delivery of $Na_V1.5$ to the ID. Indeed, our macropatch and super-resolution microscopy experiments revealed that SB2 increased the density and size of $Na_V1.5$ clusters as well as I_{Na} at the ID of WT adult murine cardiomyocytes, while $Na_V1.5$ clusters and I_{Na} at the lateral membrane remained unaffected. Interestingly, baseline I_{Na} densities were similar between WT and *Clasp2*$^{-/-}$ murine cardiomyocytes, which may be explained by a compensatory effect of the CLASP2 paralog CLASP1 in maintaining MT stabilization. In contrast, the SB2-induced increase in I_{Na} was only observed in WT cardiomyocytes and not in *Clasp2*$^{-/-}$ cells. CLASP1 was recently demonstrated to be less sensitive to GSK3β inhibition as compared to CLASP2,[76] and hence would not be able to compensate for the lack of SB2 effect on I_{Na} in *Clasp2*$^{-/-}$ cardiomyocytes. Hence, our findings establish a central role of CLASP2 in SB2-mediated enhancement of I_{Na} and $Na_V1.5$ localization at the ID.

In ACM mice, local GSK3β upregulation has been observed at the ID, with chronic SB2 treatment normalizing subcellular GSK3β distribution and reducing the incidence of ventricular arrhythmias.[77] In accordance, our *in vitro* data show that SB2 decreases the presence of GSK3β at ID of cardiomyocytes. In the compound screen during which SB2 was originally identified,[25] other compounds with GSK3β kinase inhibiting properties failed to rescue the ACM phenotype. In light of this, our current findings indicate a role for GSK3β displacement from the ID region, in addition to altered GSK3β activity, in the SB2-mediated effects on $Na_V1.5$. Post-translational modifications of tubulin, including detyrosination and acetylation, affect the MT interaction with kinesin motor proteins involved in vesicular transport and regulate movement speed of kinesin along MTs.[34,78,79] These post-translational modifications have been suggested to play a crucial role in

microdomain-specific trafficking in neurons,[80,81] in line with our current observation that SB2 increased MT detyrosination and enhanced $Na_V1.5$ trafficking preferentially to the ID. While compounds such as SB2 are likely not suitable for clinical application due to potential off-target effects, novel mechanistic insight obtained from our current study may facilitate development of novel strategies to enhance $Na_V1.5$ trafficking and increase I_{Na}. Such approaches will be of particular benefit to patients suffering from (inherited) disorders associated with an increased risk for life-threatening arrhythmias consequent to decreased $Na_V1.5/I_{Na}$ at the ID, including ACM.

In conclusion, in this study we uncover a role for the MT network, in particular the (+)-end tracking proteins EB1 and CLASP2 in mediating $Na_V1.5$ trafficking and subcellular distribution in cardiomyocytes. We demonstrate that modulation of the EB1-CLASP2 interaction increases $Na_V1.5$ and I_{Na} preferentially at the ID of cardiomyocytes in a CLASP2-dependent manner. Our findings thus identify the MT (+)-end tracking protein complex as a target for preferential modulation of $Na_V1.5$ and I_{Na} within distinct subcellular microdomains of cardiomyocytes.

Supplementary Material

Refer to Web version on PubMed Central for supplementary material.

ACKNOWLEDGEMENTS

We thank Lucía Cócera-Ortega, Shirley van Amersfoorth, and Diane Bakker (Department of Experimental Cardiology, Amsterdam UMC – location AMC) for expert technical support.

SOURCES OF FUNDING

This work was supported by grants from the Dutch Heart Foundation (CVON2012–10 PREDICT to Dr Bezzina, CVON2018–30 PREDICT2 to Drs Bezzina and Remme, CVON PREDICT Young Talent Program Fellowship to Dr Portero, and CVON2015–12 eDETECT to Dr Remme), the Netherlands Organization for Scientific Research (VICI fellowship, 016.150.610, to Dr Bezzina; VIDI fellowship, 91714371, to Dr Remme), a Foundation Leducq Transatlantic Network of Excellence (to Drs George, Burridge, MacRae, Rothenberg, Bezzina, Delmar, and Remme), and a R24 grant from the NIH (R24OD017870 to Dr MacRae). Dr Chiang was supported by an NIH T32 training grant from NHGRI (T32HG010464).

Nonstandard Abbreviations and Acronyms:

ACM	arrhythmogenic cardiomyopathy
AP	action potential
APA	action potential amplitude
APD	action potential duration
BrS	Brugada syndrome
CAR	coxsackie- and adenovirus receptor
CLASP2	CLIP-associated protein 2
CV	conduction velocity

Cx43	connexin-43
dpf	days post-fertilization
EB1	end binding protein 1
FRAP	fluorescence recovery after photobleaching
GFP	green fluorescent protein
gRNA	multi-guide RNA
GSK3β	glycogen synthase kinase 3β
hiPSC	human induced pluripotent stem cell
hiPSC-CM	human induced pluripotent stem cell-derived cardiomyocytes
hpf	hours post-fertilization
ID	intercalated disc
I_{Kr}	rapid delayed rectifier potassium current
I_{Ks}	slow delayed rectifier potassium current
I_{Na}	sodium current
$I_{outward}$	total outward current
IRES	internal ribosome entry site
KO	knockout
MDP	maximal diastolic potential
MT	microtubule
PKP2	plakophilin-2
RMP	resting membrane potential
SB2	SB216763
STORM	stochastic optical reconstruction microscopy
V_{max}	upstroke velocity
WT	wild type

REFERENCES

1. Marsman RFJ, Bezzina CR, Freiberg F, Verkerk AO, Adriaens ME, Podliesna S, Chen C, Purfürst B, Spallek B, Koopmann TT, Baczko I, Dos Remedios CG, George ALJ, Bishopric NH, Lodder EM, de Bakker JMT, Fischer R, Coronel R, Wilde AAM, Gotthardt M, Remme CA. Coxsackie and adenovirus receptor is a modifier of cardiac conduction and arrhythmia vulnerability in the setting of myocardial ischemia. J Am Coll Cardiol. 2014;63:549–559. [PubMed: 24291282]

2. Remme CA. Cardiac sodium channelopathy associated with *SCN5A* mutations: electrophysiological, molecular and genetic aspects. J Physiol. 2013;591:4099–4116. [PubMed: 23818691]

3. Shy D, Gillet L, Abriel H. Cardiac sodium channel $Na_V1.5$ distribution in myocytes via interacting proteins: The multiple pool model. Biochim Biophys Acta - Mol Cell Res. 2013;1833:886–894.

4. Vermij SH, Abriel H, van Veen TAB. Refining the molecular organization of the cardiac intercalated disc. Cardiovasc Res. 2017;113:259–275. [PubMed: 28069669]

5. Noorman M, Hakim S, Kessler E, Groeneweg JA, Cox MGPJ, Asimaki A, van Rijen HVM, van Stuijvenberg L, Chkourko H, van der Heyden MAG, Vos MA, de Jonge N, van der Smagt JJ, Dooijes D, Vink A, de Weger RA, Varro A, de Bakker JMT, Saffitz JE, Hund TJ, Mohler PJ, Delmar M, Hauer RNW, van Veen TAB. Remodeling of the cardiac sodium channel, connexin43, and plakoglobin at the intercalated disk in patients with arrhythmogenic cardiomyopathy. Hear Rhythm. 2013;10:412–419.

6. Rivaud MR, Agullo-Pascual E, Lin X, Leo-Macias A, Zhang M, Rothenberg E, Bezzina CR, Delmar M, Remme CA. Sodium channel remodeling in subcellular microdomains of murine failing cardiomyocytes. J Am Heart Assoc. 2017;6:e007622. [PubMed: 29222390]

7. Franker MAM, Hoogenraad CC. Microtubule-based transport -basic mechanisms, traffic rules and role in neurological pathogenesis. J Cell Sci. 2013;126:2319–2329. [PubMed: 23729742]

8. Galjart N Plus-end-tracking proteins and their interactions at microtubule ends. Curr Biol. 2010;20:528–537.

9. Gu C, Zhou W, Puthenveedu MA, Xu M, Jan YN, Jan LY. The microtubule plus-end tracking protein EB1 is required for K_V1 voltage-gated K^+ channel axonal targeting. Neuron. 2006;52:803–816. [PubMed: 17145502]

10. Freal A, Fassier C, Le Bras B, Bullier E, De Gois S, Hazan J, Hoogenraad CC, Couraud F. Cooperative interactions between 480 kDa Ankyrin-G and EB Proteins assemble the axon initial segment. J Neurosci. 2016;36:4421–4433. [PubMed: 27098687]

11. Leterrier C, Vacher H, Fache M-P, d'Ortoli SA, Castets F, Autillo-Touati A, Dargent B. End-binding proteins EB3 and EB1 link microtubules to ankyrin G in the axon initial segment. Proc Natl Acad Sci. 2011;108:8826–8831. [PubMed: 21551097]

12. Shaw RM, Fay AJ, Puthenveedu MA, von Zastrow M, Jan Y-N, Jan LY. Microtubule plus-end-tracking proteins target gap junctions directly from the cell interior to adherens junctions. Cell. 2007;128:547–60. [PubMed: 17289573]

13. Smyth JW, Hong T-T, Gao D, Vogan JM, Jensen BC, Fong TS, Simpson PC, Stainier DYR, Chi NC, Shaw RM. Limited forward trafficking of connexin 43 reduces cell-cell coupling in stressed human and mouse myocardium. J Clin Invest. 2010;120:266–79. [PubMed: 20038810]

14. Agullo-Pascual E, Lin X, Leo-Macias A, Zhang M, Liang F-XX, Li Z, Pfenniger A, Lübkemeier I, Keegan S, Fenyö D, Willecke K, Rothenberg E, Delmar M, Fenyo D, Willecke K, Rothenberg E, Delmar M. Super-resolution imaging reveals that loss of the C-terminus of connexin43 limits microtubule plus-end capture and $Na_V1.5$ localization at the intercalated disc. Cardiovasc Res. 2014;104:371–381. [PubMed: 25139742]

15. Chkourko HS, Guerrero-Serna G, Lin X, Darwish N, Pohlmann JR, Cook KE, Martens JR, Rothenberg E, Musa H, Delmar M. Remodeling of mechanical junctions and of microtubule-associated proteins accompany cardiac connexin43 lateralization. Hear Rhythm. 2012;9:1133–1140.e6.

16. Morrison EE, Wardleworth BN, Askham JM, Markham AF, Meredith DM. EB1, a protein which interacts with the APC tumour suppressor, is associated with the microtubule cytoskeleton throughout the cell cycle. Oncogene. 1998;17:3471–3477. [PubMed: 10030671]

17. Akhmanova A, Hoogenraad CC. Microtubule plus-end-tracking proteins: Mechanisms and functions. Curr Opin Cell Biol. 2005;17:47–54. [PubMed: 15661518]

18. Komarova Y, De Groot CO, Grigoriev I, Gouveia SM, Munteanu EL, Schober JM, Honnappa S, Buey RM, Hoogenraad CC, Dogterom M, Borisy GG, Steinmetz MO, Akhmanova A. Mammalian end binding proteins control persistent microtubule growth. J Cell Biol. 2009;184:691–706. [PubMed: 19255245]

19. Drabek K, van Ham M, Stepanova T, Draegestein K, van Horssen R, Sayas CL, Akhmanova A, ten Hagen T, Smits R, Fodde R, Grosveld F, Galjart N. Role of CLASP2 in microtubule stabilization and the regulation of persistent motility. Curr Biol. 2006;16:2259–2264. [PubMed: 17113391]
20. Aher A, Kok M, Sharma A, Rai A, Olieric N, Rodriguez-Garcia R, Katrukha EA, Weinert T, Olieric V, Kapitein LC, Steinmetz MO, Dogterom M, Akhmanova A. CLASP suppresses microtubule catastrophes through a single TOG domain. Dev Cell. 2018;46:40–58.e8. [PubMed: 29937387]
21. Mimori-Kiyosue Y, Grigoriev I, Lansbergen G, Sasaki H, Matsui C, Severin F, Galjart N, Grosveld F, Vorobjev I, Tsukita S, Akhmanova A. CLASP1 and CLASP2 bind to EB1 and regulate microtubule plus-end dynamics at the cell cortex. J Cell Biol. 2005;168:141–153. [PubMed: 15631994]
22. Watanabe T, Noritake J, Kakeno M, Matsui T, Harada T, Wang S, Itoh N, Sato K, Matsuzawa K, Iwamatsu A, Galjart N, Kaibuchi K. Phosphorylation of CLASP2 by GSK-3β regulates its interaction with IQGAP1, EB1 and microtubules. J Cell Sci. 2009;122:2969 LP–2979. [PubMed: 19638411]
23. Kumar P, Lyle KS, Gierke S, Matov A, Danuser G, Wittmann T. GSK3beta phosphorylation modulates CLASP-microtubule association and lamella microtubule attachment. J Cell Biol. 2009;184:895–908. [PubMed: 19289791]
24. Kumar P, Chimenti MS, Pemble H, Schönichen A, Thompson O, Jacobson MP, Wittmann T. Multisite phosphorylation disrupts arginine-glutamate salt bridge networks required for binding of cytoplasmic linker-associated protein 2 (CLASP2) to end-binding protein 1 (EB1). J Biol Chem. 2012;287:17050–17064. [PubMed: 22467876]
25. Asimaki A, Kapoor S, Plovie E, Arndt AK, Adams E, Liu Z, James CA, Judge DP, Calkins H, Churko J, Wu JC, MacRae CA, Kléber AG, Saffitz JE. Identification of a new modulator of the intercalated disc in a zebrafish model of arrhythmogenic cardiomyopathy. Sci Transl Med. 2014;6:240ra74–240ra74.
26. Meijer van Putten RME, Mengarelli I, Guan K, Zegers JG, van Ginneken ACG, Verkerk AO, Wilders R. Ion channelopathies in human induced pluripotent stem cell derived cardiomyocytes: a dynamic clamp study with virtual I_{K1}. Front Physiol. 2015;6:7. [PubMed: 25691870]
27. Leo-Macias A, Agullo-Pascual E, Sanchez-Alonso JL, Keegan S, Lin X, Arcos T, Liang FX, Korchev YE, Gorelik J, Fenyö D, Rothenberg E, Delmar M. Nanoscale visualization of functional adhesion/excitability nodes at the intercalated disc. Nat Commun. 2016;7.
28. Xiao H, Verdier-Pinard P, Fernandez-Fuentes N, Burd B, Angeletti R, Fiser A, Horwitz SB, Orr GA. Insights into the mechanism of microtubule stabilization by Taxol. Proc Natl Acad Sci. 2006;103:10166–10173. [PubMed: 16801540]
29. Casini S, Tan HL, Demirayak I, Remme CA, Amin AS, Scicluna BP, Chatyan H, Ruijter JM, Bezzina CR, van Ginneken ACGG, Veldkamp MW. Tubulin polymerization modifies cardiac sodium channel expression and gating. Cardiovasc Res. 2010;85:691–700. [PubMed: 19861310]
30. Hill JT, Demarest B, Gorsi B, Smith M, Yost HJ. Heart morphogenesis gene regulatory networks revealed by temporal expression analysis. Development. 2017;144:3487–3498. [PubMed: 28807900]
31. Scicluna BP, Tanck MWT, Remme CA, Beekman L, Coronel R, Wilde AAM, Bezzina CR. Quantitative trait loci for electrocardiographic parameters and arrhythmia in the mouse. J Mol Cell Cardiol. 2011;50:380–389. [PubMed: 20854825]
32. Lodder EM, Scicluna BP, Milano A, Sun AY, Tang H, Remme CA, Moerland PD, Tanck MWT, Pitt GS, Marchuk DA, Bezzina CR. Dissection of a quantitative trait locus for PR interval duration identifies Tnni3k as a novel modulator of cardiac conduction. PLoS Genet. 2012;8:e1003113. [PubMed: 23236294]
33. Remme CA, Scicluna BP, Verkerk AO, Amin AS, Van Brunschot S, Beekman L, Deneer VHM, Chevalier C, Oyama F, Miyazaki H, Nukina N, Wilders R, Escande D, Houlgatte R, Wilde AAM, Tan HL, Veldkamp MW, De Bakker JMT, Bezzina CR. Genetically determined differences in sodium current characteristics modulate conduction disease severity in mice with cardiac sodium channelopathy. Circ Res. 2009;104:1283–1292. [PubMed: 19407241]
34. Reed NA, Cai D, Blasius TL, Jih GT, Meyhofer E, Gaertig J, Verhey KJ. Microtubule acetylation promotes Kinesin-1 binding and transport. Curr Biol. 2006;16:2166–2172. [PubMed: 17084703]

35. Berrueta L, Tirnauer JS, Schuyler SC, Pellman D, Bierer BE. The APC-associated protein EB1 associates with components of the dynactin complex and cytoplasmic dynein intermediate chain. Curr Biol. 1999;9:425–428. [PubMed: 10226031]
36. Shahbazi MN, Megias D, Epifano C, Akhmanova A, Gundersen GG, Fuchs E, Perez-Moreno M. CLASP2 interacts with p120-catenin and governs microtubule dynamics at adherens junctions. J Cell Biol. 2013;203:1043–1061. [PubMed: 24368809]
37. Coghlan MP, Culbert AA, Cross DAE, Corcoran SL, Yates JW, Pearce NJ, Rausch OL, Murphy GJ, Carter PS, Roxbee Cox L, Mills D, Brown MJ, Haigh D, Ward RW, Smith DG, Murray KJ, Reith AD, Holder JC. Selective small molecule inhibitors of glycogen synthase kinase-3 modulate glycogen metabolism and gene transcription. Chem Biol. 2000;7:793–803. [PubMed: 11033082]
38. Albesa M, Ogrodnik J, Rougier J-SS, Abriel H. Regulation of the cardiac sodium channel $Na_V1.5$ by utrophin in dystrophin-deficient mice. Cardiovasc Res. 2011;89:320–328. [PubMed: 20952415]
39. Koenig X, Dysek S, Kimbacher S, Mike AK, Cervenka R, Lukacs P, Nagl K, Dang XB, Todt H, Bittner RE, Hilber K. Voltage-gated ion channel dysfunction precedes cardiomyopathy development in the dystrophic Heart. PLoS One. 2011;6:e20300. [PubMed: 21677768]
40. Shy D, Gillet L, Ogrodnik J, Albesa M, Verkerk AO, Wolswinkel R, Rougier JS, Barc J, Essers MC, Syam N, Marsman RF, Van Mil AM, Rotman S, Redon R, Bezzina CR, Remme CA, Abriel H. PDZ domain-binding motif regulates cardiomyocyte compartment-specific $Na_V1.5$ channel expression and function. Circulation. 2014;130:147–160. [PubMed: 24895455]
41. Cerrone M, Lin X, Zhang M, Agullo-Pascual E, Pfenniger A, Chkourko Gusky H, Novelli V, Kim C, Tirasawadichai T, Judge DP, Rothenberg E, Chen H-SV, Napolitano C, Priori SG, Delmar M. Missense mutations in plakophilin-2 cause sodium current deficit and associate with a Brugada syndrome phenotype. Circulation. 2014;129:1092–1103. [PubMed: 24352520]
42. Lin X, Liu N, Lu J, Zhang J, Anumonwo JMB, Isom LL, Fishman GI, Delmar M. Subcellular heterogeneity of sodium current properties in adult cardiac ventricular myocytes. Hear Rhythm. 2011;8:1923–1930.
43. Veeraraghavan R, Hoeker GS, Laviada AA, Hoagland D, Wan X, King DR, Alonso JS, Chen C, Jourdan J, Isom LL, Deschenes I, Smith JW, Gorelik J, Poelzing S, Gourdie RG. The adhesion function of the sodium channel beta subunit (β1) contributes to cardiac action potential propagation. Elife. 2018;7:e37610. [PubMed: 30106376]
44. Kucera JP, Rohr S, Rudy Y. Localization of sodium channels in intercalated disks modulates cardiac conduction. Circ Res. 2002;91:1176–82. [PubMed: 12480819]
45. Veeraraghavan R, Lin J, Hoeker GS, Keener JP, Gourdie RG, Poelzing S. Sodium channels in the Cx43 gap junction perinexus may constitute a cardiac ephapse: an experimental and modeling study. Pflugers Arch Eur J Physiol. 2015;467:2093–2105. [PubMed: 25578859]
46. Basheer WA, Shaw RM. Connexin 43 and CaV1.2 ion channel trafficking in healthy and diseased myocardium. Circ Arrhythmia Electrophysiol. 2016;9.
47. Choi WS, Khurana A, Mathur R, Viswanathan V, Steele DF, Fedida D. $K_V1.5$ surface expression is modulated by retrograde trafficking of newly endocytosed channels by the dynein motor. Circ Res. 2005;97:363–371. [PubMed: 16051887]
48. Loewen ME, Wang Z, Eldstrom J, Dehghani Zadeh A, Khurana A, Steele DF, Fedida D. Shared requirement for dynein function and intact microtubule cytoskeleton for normal surface expression of cardiac potassium channels. Am J Physiol Circ Physiol. 2009;296:H71–H83.
49. Motlagh D, Alden KJ, Russell B, García J. Sodium current modulation by a tubulin/GTP coupled process in rat neonatal cardiac myocytes. J Physiol. 2002;540:93–103. [PubMed: 11927672]
50. Nicolas CS, Park KH, El Harchi A, Camonis J, Kass RS, Escande D, Mérot J, Loussouarn G, Le Bouffant F, Baró I. I_{Ks} response to protein kinase A-dependent KCNQ1 phosphorylation requires direct interaction with microtubules. Cardiovasc Res. 2008;79:427–435. [PubMed: 18390900]
51. Yvon A-MCM, Wadsworth P, Jordan MA. Taxol suppresses dynamics of individual microtubules in living human tumor cells. Mol Biol Cell. 1999;10:947–959. [PubMed: 10198049]
52. Ligon LA, Shelly SS, Tokito M, Holzbaur ELF. The microtubule plus-end proteins EB1 and dynactin have differential effects on microtubule polymerization. Mol Biol Cell. 2003;14:1405–17. [PubMed: 12686597]

53. Milstein ML, Musa H, Balbuena DP, Anumonwo JMB, Auerbach DS, Furspan PB, Hou L, Hu B, Schumacher SM, Vaidyanathan R, Martens JR, Jalife J. Dynamic reciprocity of sodium and potassium channel expression in a macromolecular complex controls cardiac excitability and arrhythmia. Proc Natl Acad Sci. 2012;109:E2134–E2143. [PubMed: 22509027]
54. Portero V, Wilders R, Casini S, Charpentier F, Verkerk AO, Remme CA. K_V4.3 expression modulates Na_V1.5 sodium current. Front. Physiol. 2018;9:178. [PubMed: 29593552]
55. Inda MC, DeFelipe J, Muñoz A. Voltage-gated ion channels in the axon initial segment of human cortical pyramidal cells and their relationship with chandelier cells. Proc Natl Acad Sci U S A. 2006;103:2920 LP–2925. [PubMed: 16473933]
56. Melgari D, Barbier C, Dilanian G, Rücker-Martin C, Doisne N, Coulombe A, Hatem SN, Balse E. Microtubule polymerization state and clathrin-dependent internalization regulate dynamics of cardiac potassium channel: Microtubule and clathrin control of K_V1.5 channel. J Mol Cell Cardiol. 2020;144:127–139. [PubMed: 32445844]
57. Ponce-Balbuena D, Guerrero-Serna G, Valdivia CR, Caballero R, Diez-Guerra FJ, Jiménez-Vázquez EN, Ramírez RJ, Monteiro da Rocha A, Herron TJ, Campbell KF, Willis BC, Alvarado FJ, Zarzoso M, Kaur K, Pérez-Hernández M, Matamoros M, Valdivia HH, Delpón E, Jalife J. Cardiac K_{ir}2.1 and Na_V1.5 Channels Traffic Together to the Sarcolemma to Control Excitability. Circ Res. 2018;122:1501–1516. [PubMed: 29514831]
58. Lowe JS, Palygin O, Bhasin N, Hund TJ, Boyden PA, Shibata E, Anderson ME, Mohler PJ. Voltage-gated Na_V channel targeting in the heart requires an ankyrin-G-dependent cellular pathway. J Cell Biol. 2008;180:173–186. [PubMed: 18180363]
59. Mohler PJ, Rivolta I, Napolitano C, LeMaillet G, Lambert S, Priori SG, Bennett V. Na_V1.5 E1053K mutation causing Brugada syndrome blocks binding to ankyrin-G and expression of Nav1.5 on the surface of cardiomyocytes. Proc Natl Acad Sci. 2004;101:17533–17538. [PubMed: 15579534]
60. Patel DM, Dubash AD, Kreitzer G, Green KJ. Disease mutations in desmoplakin inhibit Cx43 membrane targeting mediated by desmoplakin-EB1 interactions. J Cell Biol. 2014;206:779–797. [PubMed: 25225338]
61. Allan V Motor proteins: A dynamic duo. Curr Biol. 1996;6:630–633. [PubMed: 8793279]
62. Gutstein DE, Liu FY, Meyers MB, Choo A, Fishman GI. The organization of adherens junctions and desmosomes at the cardiac intercalated disc is independent of gap junctions. J. Cell Sci. 2003;116:875–885. [PubMed: 12571285]
63. Te Riele ASJM, Agullo-Pascual E, James CA, Leo-Macias A, Cerrone M, Zhang M, Lin X, Lin B, Sobreira NL, Amat-Alarcon N, Marsman RF, Murray B, Tichnell C, van der Heijden JF, Dooijes D, van Veen TAB, Tandri H, Fowler SJ, Hauer RNW, Tomaselli G, van den Berg MP, Taylor MRG, Brun F, Sinagra G, Wilde AAM, Mestroni L, Bezzina CR, Calkins H, Peter van Tintelen J, Bu L, Delmar M, Judge DP. Multilevel analyses of SCN5A mutations in arrhythmogenic right ventricular dysplasia/cardiomyopathy suggest non-canonical mechanisms for disease pathogenesis. Cardiovasc Res. 2017;113:102–111. [PubMed: 28069705]
64. Gomes J, Finlay M, Ahmed AK, Ciaccio EJ, Asimaki A, Saffitz JE, Quarta G, Nobles M, Syrris P, Chaubey S, McKenna WJ, Tinker A, Lambiase PD. Electrophysiological abnormalities precede overt structural changes in arrhythmogenic right ventricular cardiomyopathy due to mutations in desmoplakin-A combined murine and human study. Eur Heart J. 2012;33:1942–1953. [PubMed: 22240500]
65. Rizzo S, Lodder EM, Verkerk AO, Wolswinkel R, Beekman L, Pilichou K, Basso C, Remme CA, Thiene G, Bezzina CR. Intercalated disc abnormalities, reduced Na^+ current density, and conduction slowing in desmoglein-2 mutant mice prior to cardiomyopathic changes. Cardiovasc Res. 2012;95:409–418. [PubMed: 22764152]
66. Cerrone M, Noorman M, Lin X, Chkourko H, Liang F-X, van der Nagel R, Hund T, Birchmeier W, Mohler P, van Veen TA, van Rijen HV, Delmar M. Sodium current deficit and arrhythmogenesis in a murine model of plakophilin-2 haploinsufficiency. Cardiovasc Res. 2012;95:460–468. [PubMed: 22764151]
67. Corrado D, Zorzi A, Cerrone M, Rigato I, Mongillo M, Bauce B, Delmar M. Relationship between arrhythmogenic right ventricular cardiomyopathy and Brugada syndrome: new insights from

molecular biology and clinical implications. Circ Arrhythm Electrophysiol. 2016;9:e003631. [PubMed: 26987567]

68. Corrado D, Basso C, Judge DP. Arrhythmogenic cardiomyopathy. Circ Res. 2017;121:784–802. [PubMed: 28912183]
69. Kaplan SR, Gard JJ, Protonotarios N, Tsatsopoulou A, Spiliopoulou C, Anastasakis A, Squarcioni CP, McKenna WJ, Thiene G, Basso C, Brousse N, Fontaine G, Saffitz JE. Remodeling of myocyte gap junctions in arrhythmogenic right ventricular cardiomyopathy due to a deletion in plakoglobin (Naxos disease). Hear Rhythm. 2004;1:3–11.
70. Kaplan SR, Gard JJ, Carvajal-Huerta L, Ruiz-Cabezas JC, Thiene G, Saffitz JE. Structural and molecular pathology of the heart in Carvajal syndrome. Cardiovasc Pathol. 2004;13:26–32. [PubMed: 14761782]
71. Asimaki A, Tandri H, Huang H, Halushka MK, Gautam S, Basso C, Thiene G, Tsatsopoulou A, Protonotarios N, McKenna WJ, Calkins H, Saffitz JE. A new diagnostic test for arrhythmogenic right ventricular cardiomyopathy. N Engl J Med. 2009;360:1075–84. [PubMed: 19279339]
72. Schmidt N, Basu S, Sladecek S, Gatti S, van Haren J, Treves S, Pielage J, Galjart N, Brenner HR. Agrin regulates CLASP2-mediated capture of microtubules at the neuromuscular junction synaptic membrane. J Cell Biol. 2012;198:421–437. [PubMed: 22851317]
73. Lawrence EJ, Arpag G, Norris SR, Zanic M. Human CLASP2 specifically regulates microtubule catastrophe and rescue. Mol Biol Cell. 2018;29:1168–1177. [PubMed: 29540526]
74. Stehbens SJ, Paszek M, Pemble H, Ettinger A, Gierke S, Wittmann T. CLASPs link focal-adhesion-associated microtubule capture to localized exocytosis and adhesion site turnover. Nat Cell Biol. 2014;16:558–570.
75. Soni S, Raaijmakers AJA, Raaijmakers LM, Damen JMA, van Stuijvenberg L, Vos MA, Heck AJR, van Veen TAB, Scholten A. A proteomics approach to identify new putative cardiac intercalated disk proteins. PLoS One. 2016;11:e0152231. [PubMed: 27148881]
76. Sayas CL, Basu S, van der Reijden M, Bustos-Morán E, Liz M, Sousa M, van IJcken WFJ, Avila J, Galjart N. Distinct functions for mammalian CLASP1 and −2 during neurite and axon elongation. Front. Cell. Neurosci. 2019;13:5. [PubMed: 30787869]
77. Chelko SP, Asimaki A, Andersen P, Bedja D, Amat-Alarcon N, DeMazumder D, Jasti R, MacRae CA, Leber R, Kleber AG, Saffitz JE, Judge DP. Central role for GSK3β in the pathogenesis of arrhythmogenic cardiomyopathy. JCI Insight. 2016;1:e85923.
78. Liao G, Gundersen GG. Kinesin is a candidate for cross-bridging microtubules and intermediate filaments: Selective binding of kinesin to detyrosinated tubulin and vimentin. J Biol Chem. 1998;273:9797–9803. [PubMed: 9545318]
79. Dunn S, Morrison EE, Liverpool TB, Molina-París C, Cross RA, Alonso MC, Peckham M. Differential trafficking of Kif5c on tyrosinated and detyrosinated microtubules in live cells. J Cell Sci. 2008;121:1085–1095. [PubMed: 18334549]
80. Hammond JW, Huang C-F, Kaech S, Jacobson C, Banker G, Verhey KJ. Posttranslational modifications of tubulin and the polarized transport of kinesin-1 in neurons. Mol Biol Cell. 2010;21:572–83. [PubMed: 20032309]
81. Kelliher MT, Saunders HA, Wildonger J. Microtubule control of functional architecture in neurons. Curr Opin Neurobiol. 2019;57:39–45. [PubMed: 30738328]
82. Dudek J, Cheng IF, Balleininger M, Vaz FM, Streckfuss-Bömeke K, Hübscher D, Vukotic M, Wanders RJA, Rehling P, Guan K. Cardiolipin deficiency affects respiratory chain function and organization in an induced pluripotent stem cell model of Barth syndrome. Stem Cell Res. 2013;11:806–819. [PubMed: 23792436]
83. Dambrot C, Braam SR, Tertoolen LGJ, Birket M, Atsma DE, Mummery CL. Serum supplemented culture medium masks hypertrophic phenotypes in human pluripotent stem cell derived cardiomyocytes. J Cell Mol Med. 2014;18:1509–1518. [PubMed: 24981391]
84. Tohyama S, Hattori F, Sano M, Hishiki T, Nagahata Y, Matsuura T, Hashimoto H, Suzuki T, Yamashita H, Satoh Y, Egashira T, Seki T, Muraoka N, Yamakawa H, Ohgino Y, Tanaka T, Yoichi M, Yuasa S, Murata M, Suematsu M, Fukuda K. Distinct metabolic flow enables large-scale purification of mouse and human pluripotent stem cell-derived cardiomyocytes. Cell Stem Cell. 2013;12:127–137. [PubMed: 23168164]

85. Kuo H-H, Gao X, DeKeyser J-M, Fetterman KA, Pinheiro EA, Weddle CJ, Fonoudi H, Orman MV, Romero-Tejeda M, Jouni M, Blancard M, Magdy T, Epting CL, George AL, Burridge PW. Negligible-Cost and Weekend-Free Chemically Defined Human iPSC Culture. Stem Cell Reports. 2020;14:256–270. [PubMed: 31928950]
86. Burridge PW, Holmström A, Wu JC. Chemically Defined Culture and Cardiomyocyte Differentiation of Human Pluripotent Stem Cells. Curr Protoc Hum Genet. 2015;87:21.3.1–21.3.15.
87. Burridge PW, Matsa E, Shukla P, Lin ZC, Churko JM, Ebert AD, Lan F, Diecke S, Huber B, Mordwinkin NM, Plews JR, Abilez OJ, Cui B, Gold JD, Wu JC. Chemically defined generation of human cardiomyocytes. Nat Methods. 2014;11:855–860. [PubMed: 24930130]
88. Ramakers C, Ruijter JM, Lekanne Deprez RH, Moorman AFM. Assumption-free analysis of quantitative real-time polymerase chain reaction (PCR) data. Neurosci Lett. 2003;339:62–66. [PubMed: 12618301]
89. Ruijter JM, Ramakers C, Hoogaars WMH, Karlen Y, Bakker O, van den hoff MJB, Moorman AFM. Amplification efficiency: Linking baseline and bias in the analysis of quantitative PCR data. Nucleic Acids Res. 2009;37.
90. Herfst LJ, Potet F, Bezzina CR, Groenewegen WA, Le Marec H, Hoorntje TM, Demolombe S, Baró I, Escande D, Jongsma HJ, Wilde AAM, Rook MB. Na^+ channel mutation leading to loss of function and non-progressive cardiac conduction defects. J Mol Cell Cardiol. 2003;35:549–557. [PubMed: 12738236]
91. Marangoni S, Di Resta C, Rocchetti M, Barile L, Rizzetto R, Summa A, Severi S, Sommariva E, Pappone C, Ferrari M, Benedetti S, Zaza A. A Brugada syndrome mutation (p.S216L) and its modulation by p.H558R polymorphism: standard and dynamic characterization. Cardiovasc Res. 2011;91:606–16. [PubMed: 21705349]
92. Reinhard K, Rougier J-S, Ogrodnik J, Abriel H. Electrophysiological properties of mouse and epitope-tagged human cardiac sodium channel $Na_V1.5$ expressed in HEK293 cells. F1000Research. 2013;2:48. [PubMed: 24555036]
93. Rueden CT, Schindelin J, Hiner MC, DeZonia BE, Walter AE, Arena ET, Eliceiri KW. ImageJ2: ImageJ for the next generation of scientific image data. BMC Bioinformatics. 2017;18:529. [PubMed: 29187165]
94. Pobbati A V, Mejuch T, Chakraborty S, Karatas H, Bharath SR, Guéret SM, Goy P-A, Hahne G, Pahl A, Sievers S, Guccione E, Song H, Waldmann H, Hong W. Identification of Quinolinols as Activators of TEAD-Dependent Transcription. ACS Chem Biol. 2019;14:2909–2921. [PubMed: 31742995]
95. Wu RS, Lam II, Clay H, Duong DN, Deo RC, Coughlin SR. A Rapid Method for Directed Gene Knockout for Screening in G0 Zebrafish. Dev Cell. 2018;46:112–125.e4. [PubMed: 29974860]
96. Shin JT, Pomerantsev E V, Mably JD, MacRae CA. High-resolution cardiovascular function confirms functional orthology of myocardial contractility pathways in zebrafish. Physiol Genomics. 2010;42:300–309. [PubMed: 20388839]
97. Panáková D, Werdich AA, MacRae CA. Wnt11 patterns a myocardial electrical gradient through regulation of the L-type Ca2+ channel. Nature. 2010;466:874–878. [PubMed: 20657579]
98. Drabek K, Gutiérrez L, Vermeij M, Clapes T, Patel SR, Boisset J-C, van Haren J, Pereira AL, Liu Z, Akinci U, Nikolic T, van IJcken W, van den Hout M, Meinders M, Melo C, Sambade C, Drabek D, Hendriks RW, Philipsen S, Mommaas M, Grosveld F, Maiato H, Italiano JE, Robin C, Galjart N. The microtubule plus-end tracking protein CLASP2 is required for hematopoiesis and hematopoietic stem cell maintenance. Cell Rep. 2012;2:781–788. [PubMed: 23084744]
99. Hoekstra M, Mummery CL, Wilde AAM, Bezzina CR, Verkerk AO. Induced pluripotent stem cell derived cardiomyocytes as models for cardiac arrhythmias. Front Physiol. 2012;3:346. [PubMed: 23015789]
100. Casini S, Verkerk AO, Remme CA. Human iPSC-derived cardiomyocytes for investigation of disease mechanisms and therapeutic strategies in inherited arrhythmia syndromes: strengths and limitations. Cardiovasc Drugs Ther. 2017;31:325–344. [PubMed: 28721524]

101. Veerman CC, Kosmidis G, Mummery CL, Casini S, Verkerk AO, Bellin M. Immaturity of human stem-cell-derived cardiomyocytes in culture: fatal flaw or soluble Problem? Stem Cells Dev. 2015;24:1035–1052. [PubMed: 25583389]

102. Portero V, Casini S, Hoekstra M, Verkerk AO, Mengarelli I, Belardinelli L, Rajamani S, Wilde AAM, Bezzina CR, Veldkamp MW, Remme CA. Anti-arrhythmic potential of the late sodium current inhibitor GS-458967 in murine *Scn5a*-1798insD$^{+/-}$ and human *SCN5A*-1795insD$^{+/-}$ iPSC-derived cardiomyocytes. Cardiovasc Res. 2017;113:829–838. [PubMed: 28430892]

103. Barry PH, Lynch JW. Liquid junction potentials and small cell effects in patch-clamp analysis. J Membr Biol. 1991;121:101–117. [PubMed: 1715403]

104. Tonzi P, Yin Y, Lee CWT, Rothenberg E, Huang TT. Translesion polymerase kappa-dependent DNA synthesis underlies replication fork recovery. Elife. 2018;7.

105. Huang F, Hartwich TMP, Rivera-Molina FE, Lin Y, Duim WC, Long JJ, Uchil PD, Myers JR, Baird MA, Mothes W, Davidson MW, Toomre D, Bewersdorf J. Video-rate nanoscopy using sCMOS camera–specific single-molecule localization algorithms. Nat Methods. 2013;10:653–658. [PubMed: 23708387]

106. Coelho LP. Mahotas: Open source software for scriptable computer vision. J Open Res Softw. 2013;1:e3.

NOVELTY AND SIGNIFICANCE

What Is Known?

- Loss-of-function of the cardiac sodium channel $Na_V1.5$ leads to conduction slowing, arrhythmias, and sudden cardiac death.
- $Na_V1.5$ is distributed heterogeneously across subcellular domains of the cardiomyocyte, and is enriched at the intercalated disc (ID) region.
- $Na_V1.5$ is trafficked to these subcellular regions of the cardiomyocyte through the microtubule network.

What New Information Does This Article Contribute?

- The microtubule plus-end tracking end binding protein 1 (EB1) and CLIP-associated protein 2 (CLASP2) are enriched in the ID region of cardiomyocytes.
- EB1 modulates $Na_V1.5$ trafficking, with loss of EB1 leading to reduced sodium current (I_{Na}) and conduction slowing.
- Modulation of the EB1-CLASP2 complex by the GSK3β inhibitor SB216763 affects $Na_V1.5$ and I_{Na} preferentially at the ID, and this effect is dependent on CLASP2.

Dysfunction of the sodium channel $Na_V1.5$ causes cardiac conduction slowing and arrhythmias. $Na_V1.5$ is heterogeneously distributed within distinct subcellular domains of cardiomyocytes, and is enriched at the ID region. $Na_V1.5$ is trafficked through the microtubule complex, which is known to be regulated by microtubule plus-end tracking proteins such as EB1 and CLASP2. We here demonstrate a modulatory effect of these proteins on $Na_V1.5$ trafficking, with loss of EB1 leading to reduced I_{Na} and conduction slowing. Furthermore, EB1 and CLASP2 are enriched at the ID, and enhancing their interaction using the GSK3β inhibitor SB216763 increased $Na_V1.5$ and I_{Na} preferentially at the ID, and displaced GSK3β from this region. These observations demonstrate for the first time that trafficking of $Na_V1.5$ to the ID can be modulated by targeting the EB1-CLASP2 complex, both at the molecular and pharmacological level. Our findings provide novel fundamental insight into subcellular trafficking of $Na_V1.5$, and are of potential relevance for arrhythmogenic cardiomyopathy which is associated with reduced I_{Na} and increased GSK3β at the ID. Results from this study may facilitate development of novel therapeutic strategies aimed at preventing life-threatening arrhythmias in (inherited) conditions associated with alterations in I_{Na} at the ID, including arrhythmogenic cardiomyopathy.

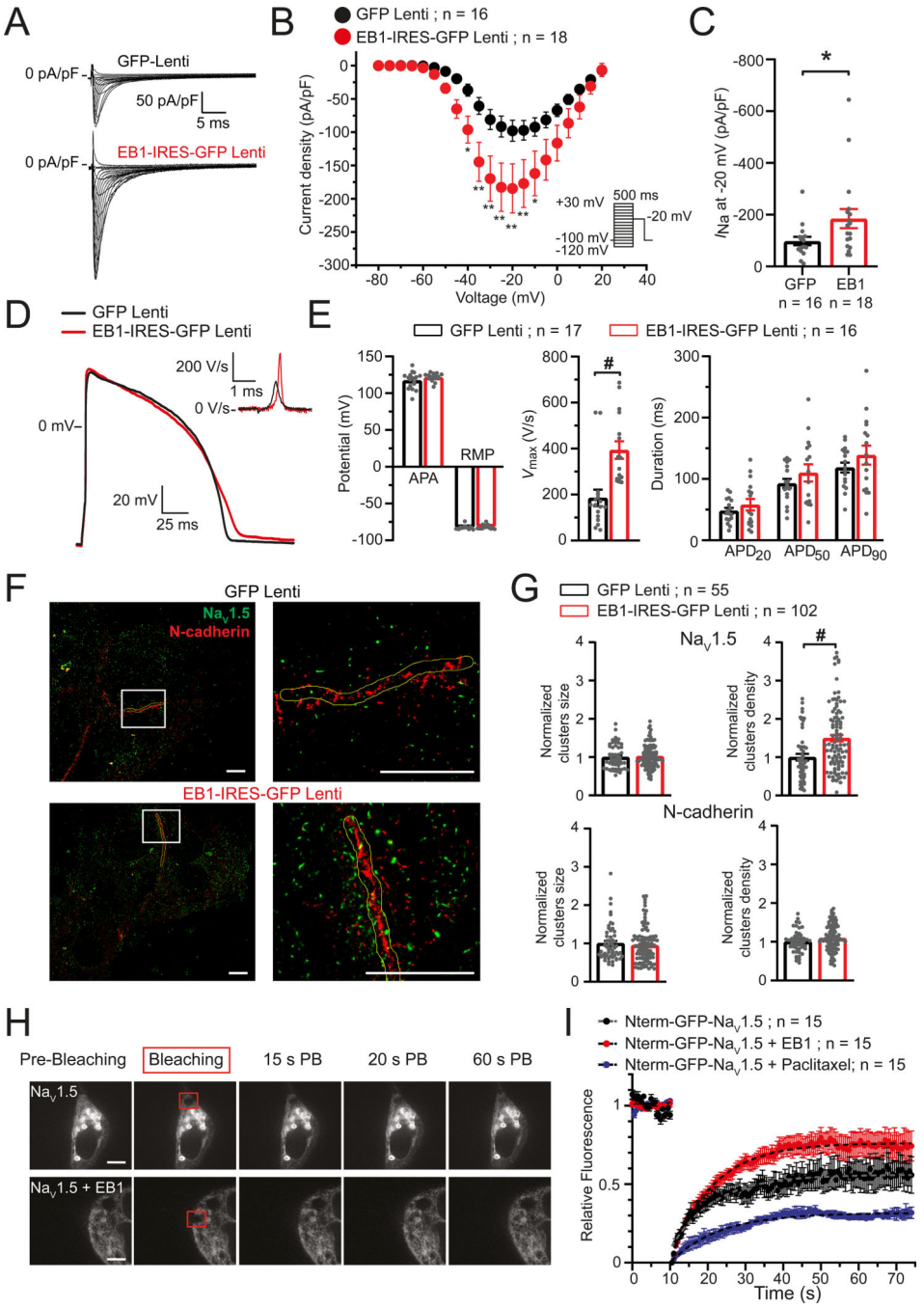

Figure 1. EB1 overexpression leads to increased sodium current density, action potential upstroke velocity and $Na_V1.5$ cluster density in hiPSC-CMs and enhanced $Na_V1.5$ trafficking in HEK293A cells.

(**A**) Representative manual whole-cell I_{Na} traces in hiPSC-CMs following lentiviral transduction with EB1-IRES-GFP or GFP-transduced hiPSC-CMs. (**B**) Average current-voltage (*I-V*) relationships of peak I_{Na} in EB1-IRES-GFP and GFP-transduced hiPSC-CMs. Inset shows voltage-clamp protocol. (**C**) Average peak I_{Na} density measured at −20 mV with or without EB1 overexpression. (**D**) Representative action potentials (APs) and maximum upstroke velocities (V_{max}) measured in hiPSC-CMs with or without EB1 overexpression at

the stimulation frequency of 1 Hz. (**E**) Average AP properties in hiPSC-CMs with or without EB1 overexpression. APA, AP amplitude, RMP, resting membrane potential, APD_{20}, APD_{50}, APD_{90}, AP duration at 20, 50, and 90% of repolarization. (**F**) Representative multi-color stochastic optical reconstruction microscopy (STORM) images showing immunoreactive signals for $Na_V1.5$ (green) and N-cadherin (red) in EB1-IRES-GFP and GFP-transduced hiPSC-CMs (scale bars: 8 μm). (**G**) $Na_V1.5$ and N-cadherin cluster characteristics (size and density) in cells with or without EB1 overexpression. All $Na_V1.5$ clusters included in the analysis have a maximum distance of 1 μm to the approximated cell end membrane. (**H**) Representative images showing GFP-$Na_V1.5$ fluorescence signal before, during and 15, 20, and 60 seconds post bleaching (PB) in HEK293A cells transfected with N-terminally GFP-fused *SCN5A* (GFP-$Na_V1.5$) with or without EB1 (scale bars: 10 μm). (**I**) Curves demonstrating the relationship between relative fluorescence and time (speed of fluorescence recovery) which were obtained in FRAP experiments in cells transfected with GFP-$Na_V1.5$ (Y_M: 0.560±0.004, k: 0.088±0.004) only or with GFP-$Na_V1.5$+EB1 (Y_M: 0.763±0.004, k: 0.091±0.002), and in cells subjected to paclitaxel treatment (10 μmol/L, 2 hours; Y_M: 0.317±0.003, k: 0.077±0.003). *$P < 0.05$, **$P < 0.01$, #$P < 0.0001$ (two-way repeated measurements ANOVA (B), Mann-Whitney U (C,E,G). n indicates number of cells measured.

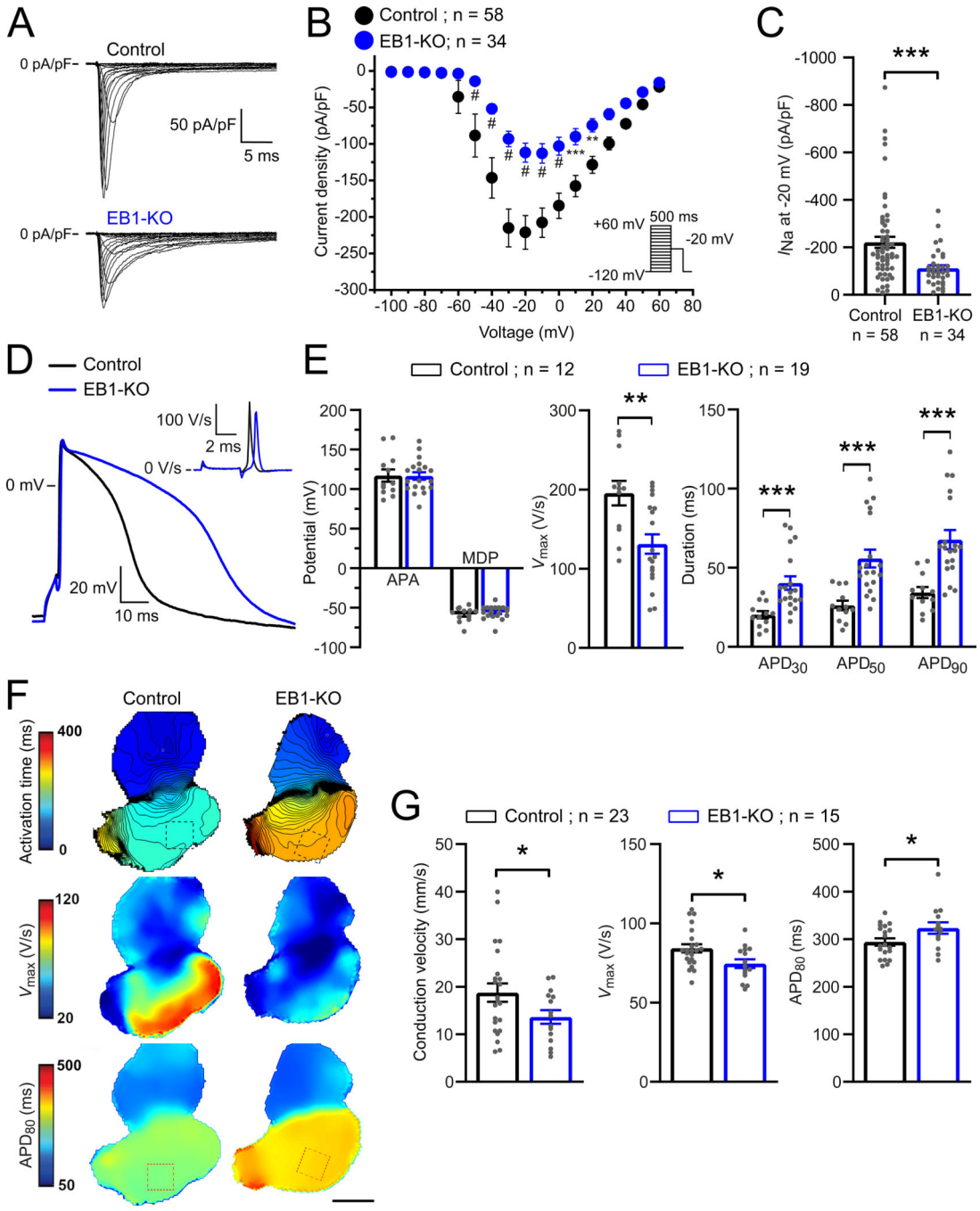

Figure 2. EB1 knockout leads to reduced sodium current density in hiPSC-CMs, slowed conduction in zebrafish ventricles, and reduced action potential upstroke velocity and increased action potential duration in both.

(**A**) Representative automated whole-cell I_{Na} traces in hiPSC-CMs in control conditions and following CRISPR/Cas9–mediated knockout of *MAPRE1* encoding EB1 (EB1-KO). (**B**) Average current-voltage (*I-V*) relationships of peak I_{Na} in control and EB1-KO hiPSC-CMs. Inset shows voltage-clamp protocol. (**C**) Average peak I_{Na} density measured at −20 mV in control and EB1-KO hiPSC-CMs. (**D**) Representative action potentials (APs) and maximum upstroke velocities (V_{max}) measured in control and EB1-KO hiPSC-CMs at the stimulation

frequency of 1 Hz. (**E**) Average AP properties in control and EB1-KO hiPSC-CMs. APA, AP amplitude, MDP, maximal diastolic potential, APD_{30}, APD_{50}, APD_{90}, AP duration at 30, 50, and 90% of repolarization. (**F**) Representative cardiac activation map (isochrone at 5 ms), V_{max} (maximal action potential upstroke velocity, dV/dt) map, and action potential duration (APD) at 80% repolarization map of hearts isolated from 3 dpf zebrafish embryos injected with tracrRNA/Cas9 and multiple gRNAs targeting *mapre1b* (EB1-KO) or tracrRNA/Cas9 without gRNA (control). The dotted squares reflect the ventricular region of interest from which parameters were measured (scale bar: 50 μm). APD measurement was performed on hearts that were paced at 80 bpm. (**G**) Average conduction velocity, V_{max}, and APD_{80} measured in EB1-KO and control hearts. $*P < 0.05$, $**P < 0.01$, $***P < 0.001$ (unpaired Student's t-test (E: APA, V_{max}; G), Mann-Whitney U (A; E: MDP), Mann-Whitney U with Holm-Bonferroni multiple testing correction (E: APD). n indicates number of cells or zebrafish hearts measured.

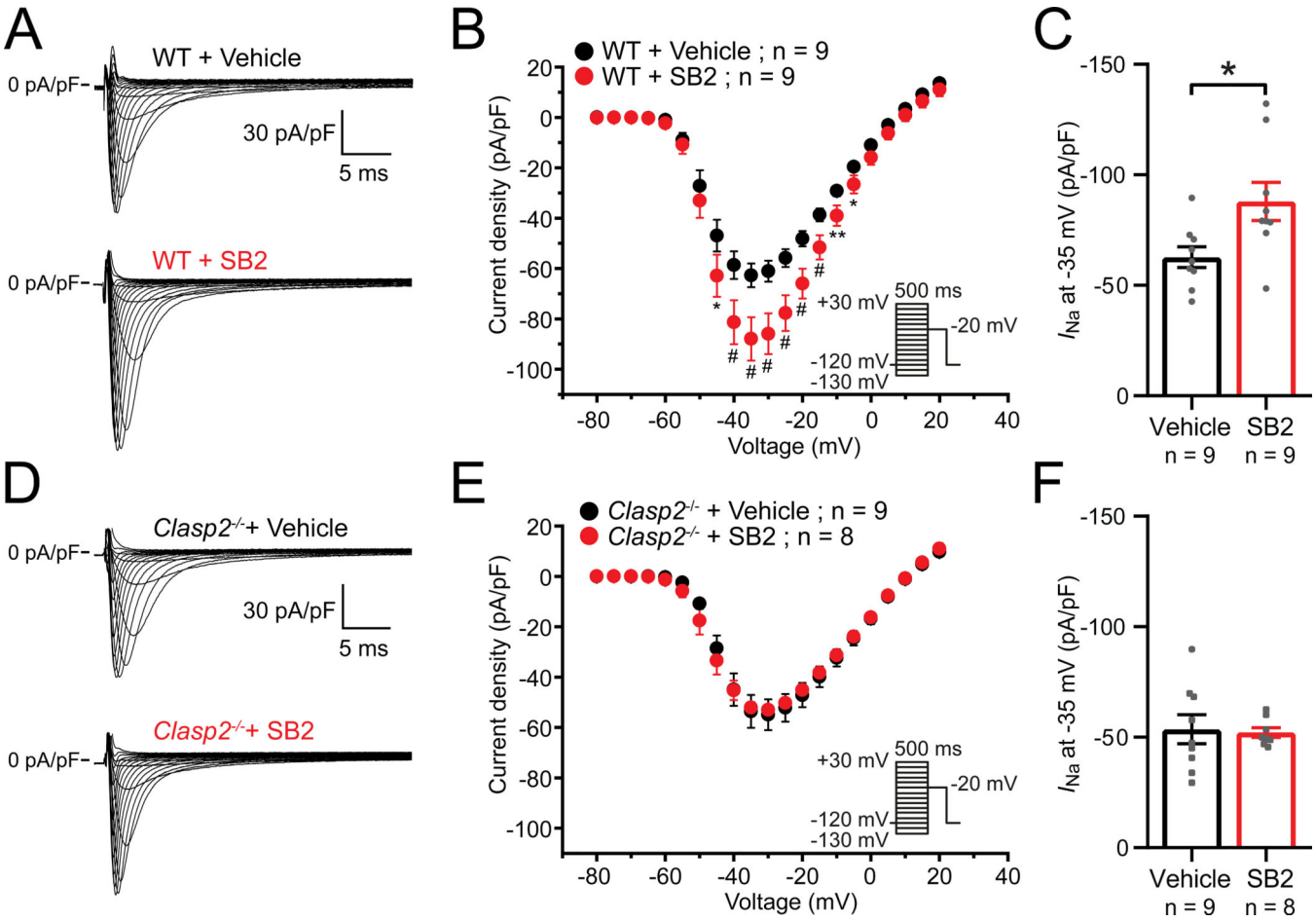

Figure 3. SB21673 (SB2) enhances I_{Na} in wild type but not *Clasp2*$^{-/-}$ mice.

(**A,D**) Representative manual whole-cell I_{Na} traces from adult murine wild type (WT, **A**) and *Clasp2*$^{-/-}$ (**D**) left ventricular cardiomyocytes after 2–3 hours incubation with vehicle or SB2. (**B,E**) Average current-voltage (*I-V*) relationships of I_{Na} in WT (**B**) and *Clasp2*$^{-/-}$ (**E**) after vehicle or SB2 treatment. Insets show voltage-clamp protocol. (**C,F**) Average peak I_{Na} density measured at −35 mV in WT (**C**) and *Clasp2*$^{-/-}$ (**F**) cardiomyocytes after vehicle or SB2 treatment. n represents the number of cells measured. Data was collected from 7 WT and 3 *Clasp2*$^{-/-}$ mice. *$P < 0.05$, **$P < 0.01$, #$P < 0.0001$ (two-way repeated measurements ANOVA, followed by a Holm-Sidak post-hoc test (B), unpaired Student's t-test (C)).

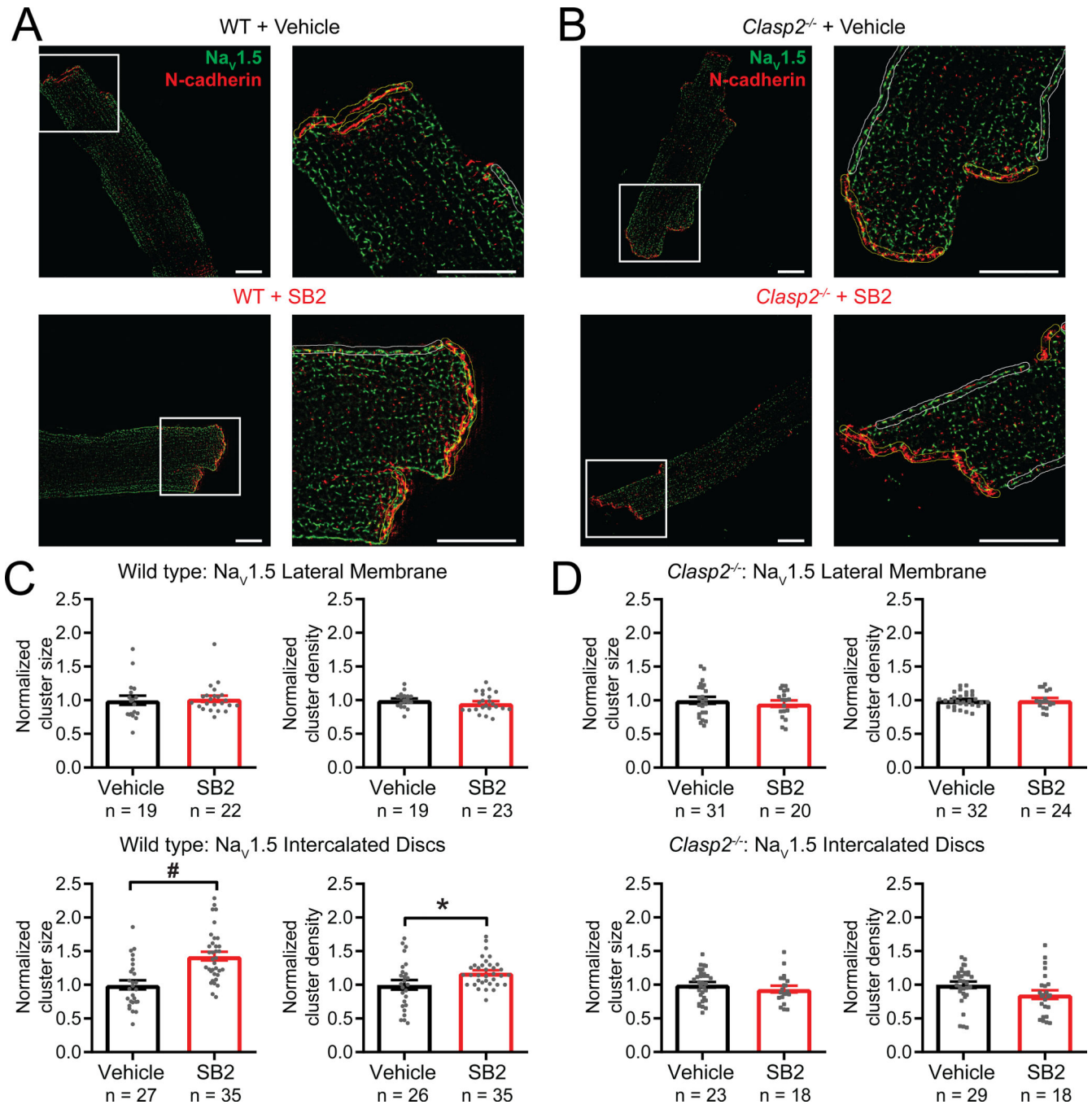

Figure 4. SB21673 (SB2) treatment results in increased Na$_V$1.5 localization at the intercalated discs (ID) in wild type but not *Clasp2*$^{-/-}$ mice.

Representative multi-color STORM images showing immunofluorescently labelled Na$_V$1.5 (green) and N-cadherin (red) after 2–3 hours of incubation with either vehicle or SB2 in wild type (WT) (**A**) and (**B**) *Clasp2*$^{-/-}$ cardiomyocytes (scale bars: 10 μm). Quantification of Na$_V$1.5 cluster size and cluster density at the lateral membrane and ID of (**C**) WT and (**D**) *Clasp2*$^{-/-}$ cardiomyocytes after 2–3 hours of incubation with vehicle or SB2. n represents

the number of cells measured. Data was collected from 3 WT and 3 *Clasp2*$^{-/-}$ mice. *P < 0.05, #P < 0.0001 (unpaired Student's t-test).

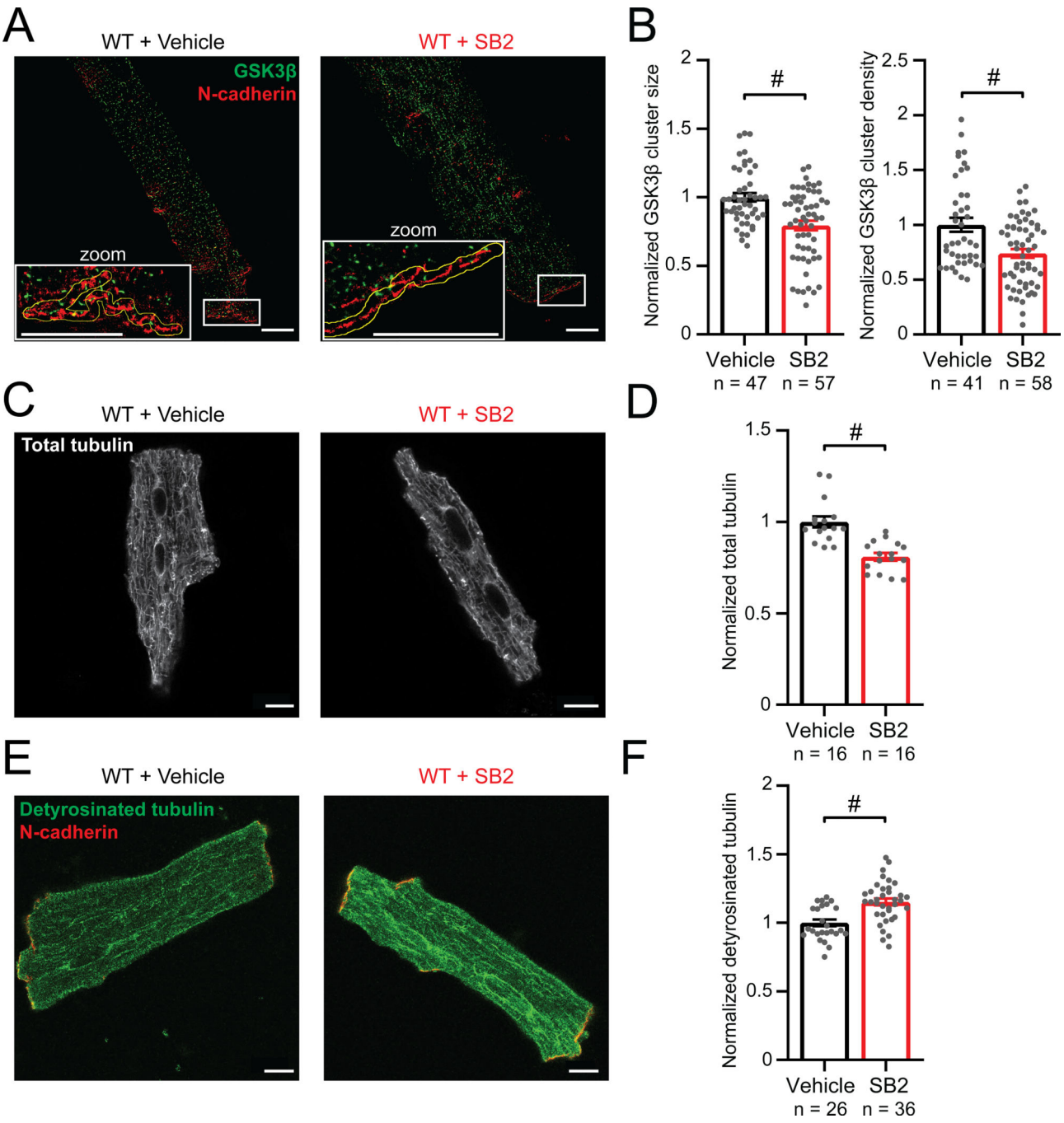

Figure 5. SB21673 (SB2) affects GSK3β localization and microtubule characteristics.

(**A**) Representative multi-color STORM images of adult murine wild type (WT) showing labelled GSK3β (green) and N-cadherin (red) after 2–3 hours of incubation with either vehicle or SB2, and (**B**) average GSK3β cluster size and cluster. (**C**) Typical maximum intensity projections of stacked confocal images showing immunolabeled tubulin in adult WT murine cardiomyocytes after incubation with either vehicle of SB2, and (**D**) average total tubulin levels. (**E**) Typical maximum intensity projections of stacked confocal images showing immunolabeled detyrosinated tubulin (green) and N-cadherin (red) in adult WT

murine cardiomyocytes after 2–3 hours of incubation with vehicle or SB2, (**F**) and average detyrosinated tubulin levels located near N-cadherin. Scale bars: 10 μm; n represents the number of cells measured. Data was collected from 4 (GSK3β dataset) and 2 (microtubule quantification) WT mice. #$P < 0.0001$ (Mann-Whitney U test (B,D,F)).

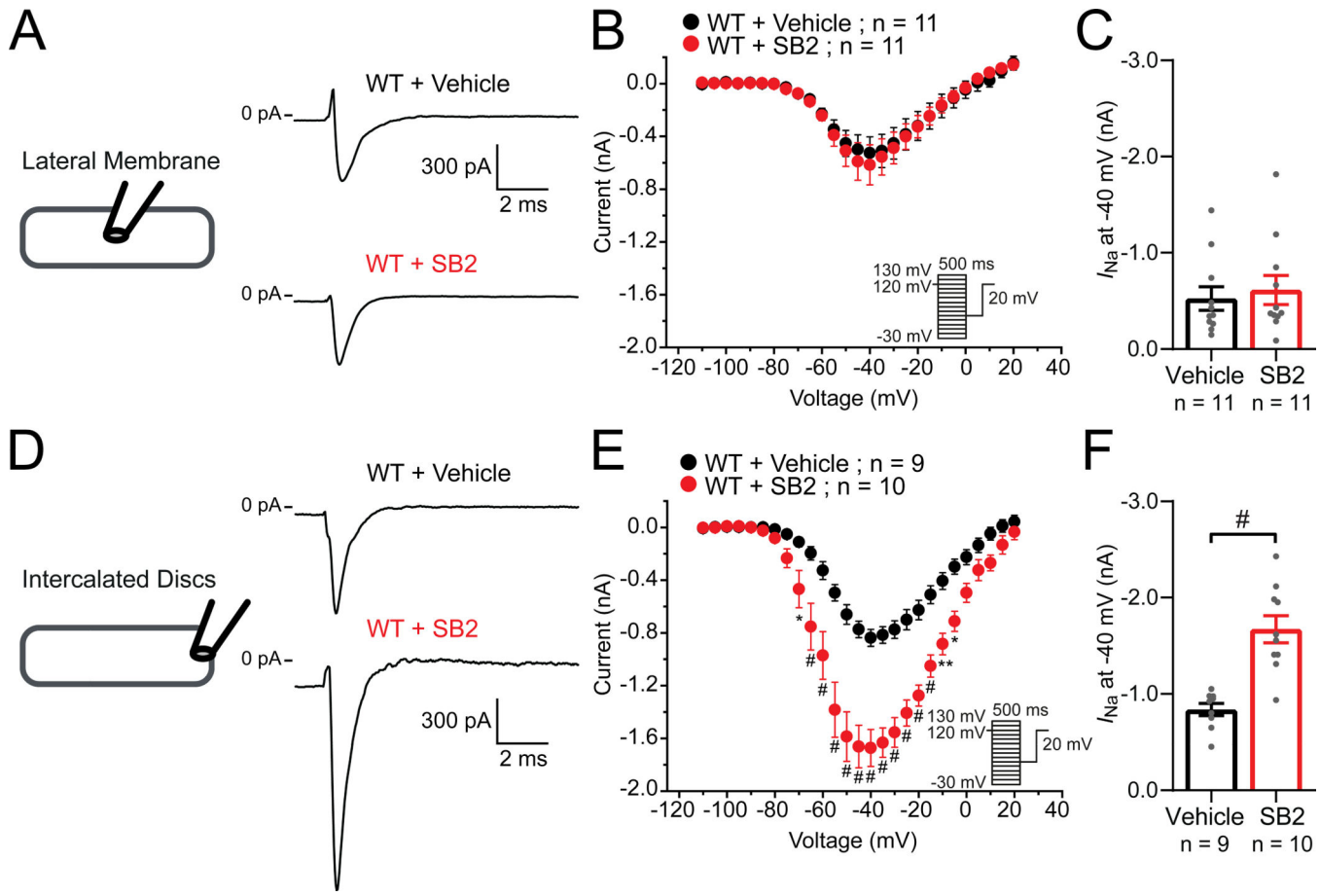

Figure 6. SB21673 (SB2) enhances I_{Na} at the intercalated disc (ID) region of adult WT murine cardiomyocytes.

(**A,D**) Schematic drawing of pipette placement (left), and representative macropatch traces (right) of I_{Na} measured at the lateral membrane (**A**) and ID region (**D**) at −40 mV after 2–3 hours of incubation with vehicle or SB2. (**B,E**) Average current-voltage (*I-V*) relationship of I_{Na} generated at the lateral membrane (**B**) and ID region (**E**) of cardiomyocytes upon vehicle or SB2 treatment. Insets show voltage-clamp protocol. (**C,F**) Peak I_{Na} generated at −40 mV at the lateral membrane (**C**) and ID region (**F**) of cardiomyocytes upon vehicle or SB2 treatment. Lateral membrane I_{Na} was measured in 8 WT mice, while ID region data was generated in 5 animals. n represents the number of cells measured. $*P < 0.05$, $**P < 0.01$, $\#P < 0.0001$ (two-way repeated measurements ANOVA, followed by a Holm-Sidak post-hoc test (E), unpaired Student's t-test (F)).

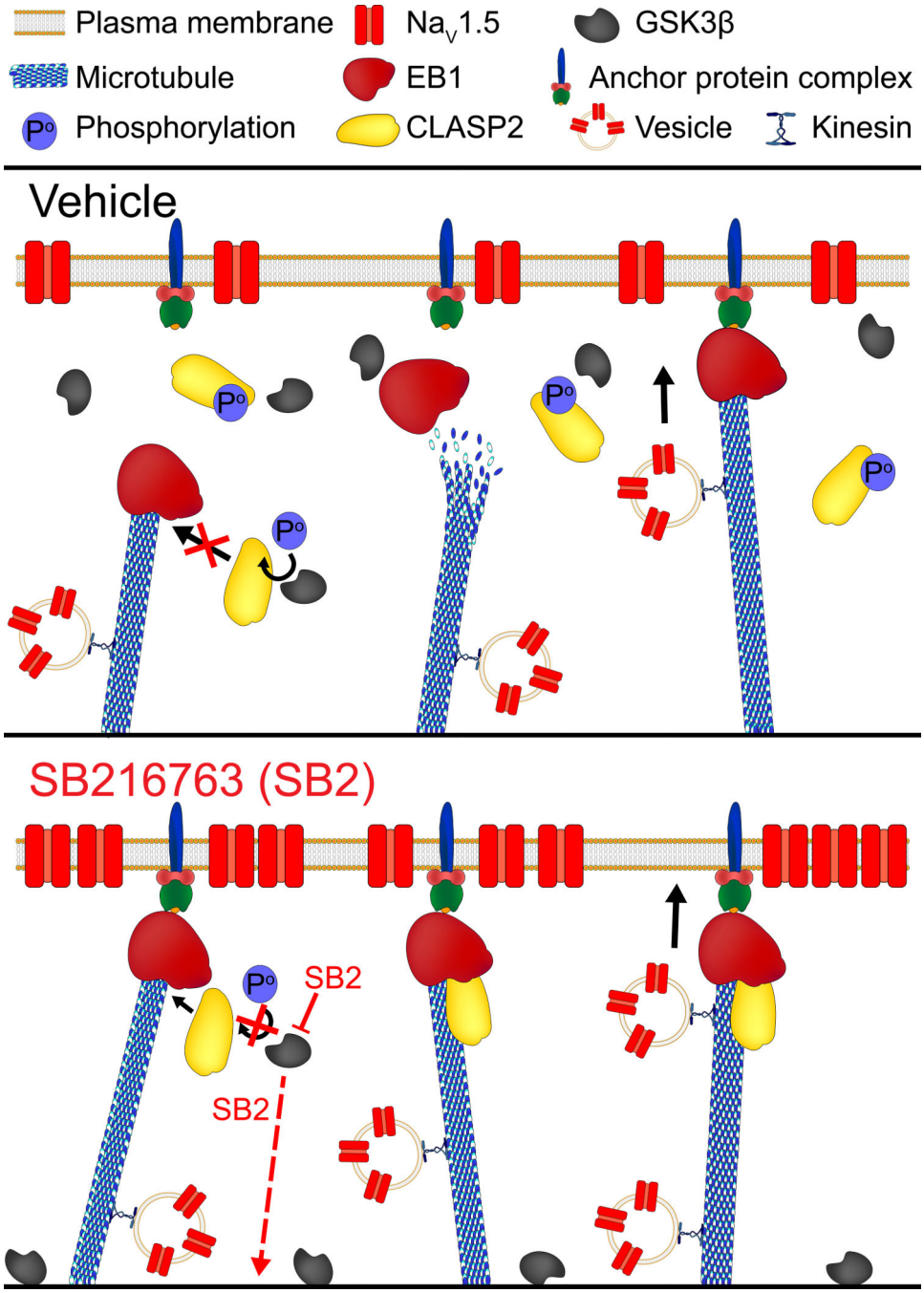

Figure 7. Proposed mechanism of the modulatory effect of SB2 on Na$_V$1.5 delivery to the intercalated disc (ID).

The microtubule (+)-end tracking proteins EB1 and CLASP2 both prevent microtubule breakdown and are able to interact with anchoring proteins located in the cell membrane. SB2 prevents GSK3β-mediated CLASP2 phosphorylation, thereby enhancing EB1-CLASP2-microtubule interactions, resulting in increased Na$_V$1.5 delivery at the ID of cardiomyocytes.